The description of N_2 and F_2 potential energy surfaces using multireference coupled cluster theory

Cite as: J. Chem. Phys. **86**, 887 (1987); https://doi.org/10.1063/1.452291
Submitted: 22 January 1986 . Accepted: 01 October 1986 . Published Online: 31 August 1998

William D. Laidig, Paul Saxe, and Rodney J. Bartlett

The description of N_2 and F_2 potential energy surfaces using multireference coupled cluster theory[a)]

William D. Laidig, Paul Saxe,[b)] and Rodney J. Bartlett[c)]
Quantum Theory Project, University of Florida, Gainesville, Florida 32611

(Received 22 January 1986; accepted 1 October 1986)

The ground state potential energy surfaces (PES's) for diatomic nitrogen and fluorine are examined using a version of our recently published linearized multireference coupled cluster method (MR-LCCM). Comparison calculations employing a variety of standard *ab initio* techniques such as single reference configuration interaction singles and doubles (CISD), many-body perturbation theory (MBPT), coupled cluster single and doubles (CCSD), and multireference (MR)-CISD were also performed. In addition, the PES's were also investigated using the newly developed CCSDT-1 method, which includes the dominant effect of $\hat{T}_3$. These single reference procedures fail in various ways (with the possible exception of the CCSDT-1 method), while the MR-LCCM method is shown to compare favorably to the more traditional MR-CI techniques. Like the MR-CIs, the MR-LCCM energy curves dissociate correctly and the two are nearly parallel.

I. INTRODUCTION

The inability of most single-reference procedures to qualitatively describe bond breaking severely limits their general applicability. Restricted-Hartree–Fock (RHF) based methods cannot be easily extended to remove these defects and even if extensive "dynamical" correlation is included the fragments may still not separate correctly. For example, even at the configuration interaction singles, doubles, triples, and quadruples (CISDTQ) level of theory the energy required to symmetrically break the O–H bond in water was found to be in error by over 2 kcal/mol relative to the corresponding full-CI result,[1] and many-body perturbation theory (MBPT) calculations in general become divergent as the fragments separate.[1,2] Unrestricted-Hartree–Fock (UHF) wave functions usually separate correctly and, consequently, correlated methods employing such reference functions generally yield good dissociation energies. However, UHF wave functions can be quite spin contaminated especially in the intermediate bond-breaking region and as a result spurious barriers are often found in even highly correlated calculations, with spin projection only a partial remedy.

In CI theory these difficulties have been overcome by adopting a more sophisticated zeroth-order reference, which is typically a multiconfiguration SCF (MCSCF) function.[3–6] If the MCSCF wave function is chosen with sufficient care to include the important configurations along the entire bond-breaking path then the so-called "nondynamical" correlation is introduced and quantitative accuracy within the basis set can often be achieved by just adding additional single and double excitations from Ψ_{MCSCF} to the CI to introduce "dynamical" correlation.

In contrast to CI, the use of multireference (MR) techniques in MBPT and coupled-cluster (CC) theory is far less developed. This is primarily because CI, due to its simplicity, was the first correlated method to be implemented and modification to handle multiple references is relatively straightforward. Nonetheless, much work is being done in several laboratories to adapt MR techniques to both MBPT[7–14] and CC,[8,15–21] though to date only a few modest sized calculations have been carried out employing any of these MBPT[22–26] or CC[1,18,19,27,28] methods.

As the first step in implementing a complete multireference coupled-cluster singles and doubles (MR-CCSD) theory we recently introduced a linearized version which we call the multireference linearized coupled-cluster method (MR-LCCM).[1] This complete-active-space (CAS) MCSCF reference-based method was designed to compete favorably with the traditional MR-CISD approach, and, hence, for calculations possessing identical configuration lists the two methods require nearly identical amounts of computational time and storage space. The deficiencies of the single-reference linearized CCSD (L-CCSD) theory are well known when near degeneracies are present.[2] However, in the absence of such degeneracies L-CCSD typically yields good energies, fortuitously closer to the exact result than the corresponding CISD calculations.[29,30] Analogously, the MR-LCCM energies are expected to lie closer to the full CI for those regions of the PES where the near degeneracy effects have been absorbed into the MCSCF reference. In addition, CC theory has the advantage of size extensivity[2] which, e.g., is important in determining accurate dissociation energies and in proper scaling for larger molecules.

In our initial investigation of the MR-LCCM method[1] we studied two model MR systems: symmetric insertion of Be into H_2 and symmetric bond dissociation in water. For both systems the results of a number of correlated methods including MR-CISD, MR-LCCM, and full-CI were computed at several distinct geometries. Overall, the MR-LCCM method performed better than any of the single-reference MBPT/CC methods and compared well with MR-CISD (though conflicting results were obtained for the two systems as to which method was "best"). However, both

[a)] This work is supported by the U. S. Office of Naval Research.
[b)] Permanent address: Los Alamos National Laboratory, Los Alamos, New Mexico 87544.
[c)] Guggenheim Fellow. Author for correspondence.

 0021-9606/87/020887-21$02.10

preliminary studies employed small [double-zeta (DZ)] basis sets and the reference space was limited to at most 12 configurations.

In the present investigation, the applicability of studying bond breaking via the MR-LCCM approach is tested on ground-state F_2 and N_2. These two molecules were chosen because they are both relatively small yet possess potential energy curves that are difficult to correctly describe. In F_2, for instance, the UHF potential curve is not bound[31] and even at the valence-space CAS-MCSCF level of theory[3] the binding energy is found to be less than half the limiting value. N_2, by nature of its triple bond, is very difficult to properly separate requiring at least some sixfold excitations in the wave function for correct dissociation. In contrast to our previous MR-LCCM work, this investigation adopted more realistically sized basis sets [larger than DZ plus polarization (DZP)] since basis sets of this size are typically employed in correlated calculations. In addition, the maximum size of the MR space has been increased from 12 configurations (in our earlier water study) to 176 configurations (in the present N_2 work).

Since full-CI calculations are unfeasible for such large systems the quality of the MR-LCCM F_2 and N_2 PES's is estimated through comparison with PES's obtained using more traditional techniques. For this purpose we computed single-reference potential curves at the CISD, CCSD, and MBPT through fourth-order levels of theory. In addition, dissociation curves were computed using the new CCSDT-1 method[32] which approximates the effect of iteratively including $\hat{T}_3$ in CCSD calculations. The MR-LCCM results were also compared with the analogous MR-CISD calculations as well as to the MCSCF curves themselves. From these curves various spectroscopic constants were obtained including the harmonic frequencies and anharmonicities in addition to accurate vibrational energy differences obtained through numerical solution of the nuclear Schrödinger equation. Direct comparison with experiment is kept to a minimum since the basis set, while moderately large, is not adequate for reproducing the experimental PES to sufficient accuracy at the fully correlated limit, yet comparisons among the different methods are highly informative.

After a brief discussion of the MR-LCCM theory in Sec. II, general computational details are presented in Sec. III, with numerical results for F_2 in Secs. IV and V, and N_2 in Secs. VI and VII.

II. THEORY

In our previous publication[1] the MR-LCCM method was derived starting from the MR-CC ansatz of Jeziorski and Monkhorst.[16] However, in the present work the same final equations will be derived in a simpler and more straightforward fashion using a slightly different ansatz.

Define two indempotent, self-adjoint, and mutually exclusive projection operators,

$$\hat{P}=\sum_{\mu}\hat{P}_{\mu}=\sum_{\mu}|\Phi_{\mu}\rangle\langle\Phi_{\mu}| \tag{1}$$

and

$$\hat{Q}=\hat{1}-\hat{P}=\sum_{r}|\Phi_{r}\rangle\langle\Phi_{r}|, \tag{2}$$

where $\{\Phi_{\mu}\}$ and $\{\Phi_{r}\}$ are sets of orthonormal configurations that span the reference space P and its orthogonal space Q, respectively. We also define a second set of othonormal functions that span the P space $\{\Psi_{\mu}^{0}\}$ where Ψ_{1}^{0} is chosen to be the MCSCF function for the state of interest. That is,

$$\Psi_{\nu}^{0}=\sum_{\mu}c_{\mu\nu}|\Phi_{\mu}\rangle \tag{3}$$

and

$$\Psi_{\mathrm{MC}}=\Psi_{1}^{0}=\sum_{\mu}c_{\mu 1}|\Phi_{\mu}\rangle. \tag{4}$$

For convenience in these initial studies, we require the space P to be complete, although for our purposes an SOGVB choice would have the same properties. That is, if the orbitals are partitioned into three groups: core, active, and virtual where the core orbitals are always doubly occupied, the active orbitals have variable occupancy (not 0 or 2 for at least one configuration), and the virtual orbitals are always unoccupied in all reference configurations, the P space contains all excitations exclusively within the active space.

In analogy to single reference CC theory the exact wave function Ψ can be represented as

$$\Psi=\exp(\hat{T})|\Psi_{\mathrm{MC}}\rangle, \tag{5}$$

where the cluster operator $\hat{T}$ is defined as

$$\hat{T}=\sum_{r,\alpha}t_{r}^{\alpha}\alpha^{+}r+\sum_{\substack{\alpha>\beta\\ r>s}}t_{rs}^{\alpha\beta}\alpha^{+}r\beta^{+}s \tag{6}$$

and the indices $r,s,t,\ldots$ and $\alpha,\beta,\gamma,\ldots$ range over all core and active orbitals and all virtual and active orbitals, respectively. As a first approximation we also exclude terms involving solely active to active excitations. The reason for excluding these fully internal excitations will become apparent in the discussion that follows. Substituting Eq. (5) into the Schrödinger equation, $H\Psi=E\Psi$, and left multiplying by $\exp(-\hat{T})$ yields

$$\exp(-\hat{T})\hat{H}\exp(\hat{T})|\Psi_{\mathrm{MC}}\rangle=E|\Psi_{\mathrm{MC}}\rangle. \tag{7}$$

Projecting Eq. (7) on the left with $\langle\Psi_{\mathrm{MC}}|$ yields an expression for the energy E as a function of $\hat{T}$,

$$\langle\Psi_{\mathrm{MC}}|\exp(-\hat{T})\hat{H}\exp(\hat{T})|\Psi_{\mathrm{MC}}\rangle=E \tag{8}$$

and left projecting onto the set of $\langle\Phi_{r}|$, $r\in Q$ yields the set of equations,

$$\langle\Phi_{r}|\exp(-\hat{T})\hat{H}\exp(\hat{T})|\Psi_{\mathrm{MC}}\rangle=0 \tag{9}$$

which define the coefficients t. Here, $\{\Phi_{r}\}$ consists of nonredundant single and double excitations from all references in Ψ_{MC}.

It should be pointed out that solving Eqs. (8) and (9) exactly, while excluding the all internal excitations from $\hat{T}$, does not yield the exact wave function Ψ. This is because Eqs. (8) and (9) contain no mechanism for changing the relative weights of the configurations $|\Phi_{\mu}\rangle$, $\mu\in P$ in Eq. (3). The exact Ψ can be expressed as $\Psi=\exp(\hat{T})\ |\Psi_{1}^{0\prime}\rangle$ where $|\Psi_{1}^{0\prime}\rangle=\Sigma_{\mu}c_{\mu 1}^{\prime}|\Phi_{\mu}\rangle$ and the internal excitations are justifiably omitted from $\hat{T}$ provided an additional set of equations

are then solved to determine the exact P space coefficients, $\mathbf{c}'$. This is normally accomplished by diagonalization of an effective Hamiltonian. Equivalently, the other $P-1$ linear combinations of $\{\Phi_\mu\}$ orthogonal to Ψ_i^0 would have to be introduced into the Q space. Formally then, an iterative procedure can be envisioned whereby Eqs. (8) and (9) are first solved followed by the solution of $n_p - 1$ additional equations to determine improved P space coefficients $\mathbf{c}$, where n_p is the number of configurations in the P space. Then Eqs. (8) and (9) are again solved, however now $|\Psi_{\rm MC}\rangle$ is replaced by the new trial wave function constructed from the modified $\mathbf{c}$ coefficients. This process would be repeated until the $\mathbf{c}$ coefficients were converged.

In our current MR-LCCM method we never modify the P space coefficients and, therefore, this method is analogous to truncating the iterative procedure described above after the first step. However, since the initial P space coefficients are determined via the CAS-MCSCF procedure we anticipate that the use of this approximation will lead to a relatively small error, since the CAS wave function is chosen to contain the dominant configurations with the MCSCF procedure determining the optimum weighting. If this is the case, the addition of the secondary, Q space configurations should mainly change the weight of the total MCSCF reference function while only slightly modifying the relative weights of its component configurations.

Expanding the exponentials in Eq. (8) using the Baker–Campbell–Hausdorff commutator expansion yields

$$E = \langle\Psi_{\rm MC}|\hat{H}|\Psi_{\rm MC}\rangle + \langle\Psi_{\rm MC}|[\hat{H},\hat{T}]|\Psi_{\rm MC}\rangle + \tfrac{1}{2}\langle\Psi_{\rm MC}|[[\hat{H},\hat{T}],\hat{T}]|\Psi_{\rm MC}\rangle + \cdots. \quad (10)$$

Since for these initial MR-CC investigations we are adopting a linearized theory only the first two terms are retained leaving

$$E = E_{\rm MC} + \langle\Psi_{\rm MC}|\hat{H}\hat{T}|\Psi_{\rm MC}\rangle - \langle\Psi_{\rm MC}|\hat{T}\hat{H}|\Psi_{\rm MC}\rangle, \quad (11)$$

after the commutator has been expanded. This expression can be simplified to

$$E = E_{\rm MC} + \langle\Psi_{\rm MC}|\hat{H}\hat{T}|\Psi_{\rm MC}\rangle, \quad (12)$$

since the third term on the right-hand side of Eq. (11) is zero because $\langle\Psi_{\rm MC}|\hat{T}\hat{H}|\Psi_{\rm MC}\rangle = \langle\hat{T}^{+}\Psi_{\rm MC}|\hat{H}|\Psi_{\rm MC}\rangle$ and $\hat{T}^{+}\Psi_{\rm MC} = 0$ since no internal to internal excitations are allowed in $\hat{T}$, i.e., the MCSCF wave function is complete. Unlike standard CC/MBPT approaches, in the following we choose to work exclusively in the spin-adapted configuration space description. Hence, we introduce the resolution of the identity in terms of orthonormal configurations $1 = \Sigma_{\mu\in P}|\Phi_\mu\rangle\langle\Phi_\mu + \Sigma_{r\in Q}|\Phi_r\rangle\langle\Phi_r|$ into Eq. (12) to give

$$E = E_{\rm MC} + \sum_{\Phi_\mu\in P}\langle\Psi_{\rm MC}|\hat{H}|\Phi_\mu\rangle\langle\Phi_\mu|\hat{T}|\Psi_{\rm MC}\rangle + \sum_{\Phi_r\in Q}\langle\Psi_{\rm MC}|H|\Phi_r\rangle\langle\Phi_r|T|\Psi_{\rm MC}\rangle. \quad (13)$$

The second term on the right-hand side of Eq. (13) is also zero since $\langle\Phi_\mu|\hat{T}|\Psi_{\rm MC}\rangle = 0$ due to our definition of $\hat{T}$ and the completeness of $\Psi_{\rm MC}$. Therefore, the final energy equation written in matrix notation is

$$E = E_{\rm MC} + \mathbf{H}_{Q,\rm MC}^{+}\mathbf{T}_{Q,\rm MC}. \quad (14)$$

To solve Eq. (14) an equivalent matrix equation must be derived for $\mathbf{T}_{Q,\rm MC}$. Expanding the exponentials in Eq. (9) yields

$$\langle\Phi_r|\hat{T}|\Psi_{\rm MC}\rangle + \langle\Phi_r|[\hat{H},\hat{T}]|\Psi_{\rm MC}\rangle + \tfrac{1}{2}\langle\Phi_r|[[\hat{H},\hat{T}],\hat{T}]|\Psi_{\rm MC}\rangle + \cdots \quad (15)$$

for all $r\in Q$. Truncating Eq. (15) to first order in $\hat{T}$, expanding the commutator and inserting the identity resolution between $\hat{H}\hat{T}$ and $\hat{T}\hat{H}$ we obtain for all $r\in Q$,

$$\langle\Phi_r|\hat{H}|\Psi_{\rm MC}\rangle + \sum_{\Psi_\mu^0\in P}\langle\Phi_r|\hat{H}|\Psi_\mu^0\rangle\langle\Psi_\mu^0|\hat{T}|\Psi_{\rm MC}\rangle + \sum_{\Phi_s\in Q}\langle\Phi_r|\hat{H}|\Phi_s\rangle\langle\Phi_s|\hat{T}|\Phi_{\rm MC}\rangle - \sum_{\Psi_\mu^0\in P}\langle\Phi_r|\hat{T}|\Psi_\mu^0\rangle\langle\Psi_\mu^0|\hat{H}|\Psi_{\rm MC}\rangle - \sum_{\Phi_s\in Q}\langle\Phi_r|\hat{T}|\Phi_s\rangle\langle\Phi_s|\hat{H}|\Psi_{\rm MC}\rangle = 0. \quad (16)$$

The second term on the left-hand side of Eq. (16) is zero and $\langle\Psi_\mu|\hat{H}|\Psi_{\rm MC}\rangle$ in the fourth term is $\delta_{\mu,\rm MC}E_{\rm MC}$ due to completeness of the MCSCF. In matrix form, then, the equation for $\hat{T}$ is

$$\mathbf{H}_{Q,\rm MC} - E_{\rm MC}\mathbf{T}_{Q,\rm MC} - \mathbf{T}_{Q,Q}\mathbf{H}_{Q,\rm MC} + \mathbf{H}_{Q,Q}\mathbf{T}_{Q,\rm MC} = \mathbf{0}. \quad (17)$$

Our last approximation is to drop the $\mathbf{T}_{Q,Q}\mathbf{H}_{Q,\rm MC}$ term in Eq. (16). The justification for this is detailed in the Appendix. Using this approximation Eq. (17) simplifies to

$$(\mathbf{H}_{Q,Q} - E_{\rm MC}\mathbf{1}_{Q,Q})\mathbf{T}_{Q,\rm MC} = -\mathbf{H}_{Q,\rm MC}. \quad (18)$$

This linear equation for the T amplitudes along with the energy expression [Eq. (14)] constitutes the basis for the multireference linearized coupled cluster method (MR-LCCM).

III. COMPUTATIONAL CONSIDERATIONS

The matrices $\mathbf{H}_{Q,\rm MC}$ and $\mathbf{H}_{Q,Q}$ in our implementation are computed in a spin adapted configuration basis obtained using the graphical unitary group approach (GUGA) formalism.[33] In fact our MR-LCCM program was obtained from a relatively simple and straightforward modification of an existing GUGA-CI program, the shape-driven GUGA program of Saxe *et al.* (SDGUGA).[16] This brings up the two main points we wish to stress in this section: First, that the capacity to perform MR-LCCM calculations can be relatively easily added to most existing CI programs and, second, that equivalent MR-CISD and MR-LCCM calculations (i.e., those employing identical configuration lists) require virtually the same amount of CPU time and similar amounts of external disk space.

To modify an existing CI code to perform MR-LCCM calculations requires three changes: The Hamiltonian submatrices $\mathbf{H}_{P,P}$ and $\mathbf{H}_{Q,P}$ must be constructed efficiently; $\mathbf{H}_{P,P}$ must be diagonalized via $\mathbf{V}^{+}\mathbf{H}_{P,P}\mathbf{V}$ to yield $E_{\rm MC}$ and $\mathbf{H}_{Q,P}$ transformed to $\mathbf{H}'_{Q,P}$ where $\mathbf{H}'_{Q,P} = \mathbf{H}_{Q,P}\mathbf{V}$; and the diagonalization procedure must be replaced by a procedure to solve a large system of linear equations.

Let us examine these points one by one. For CI pro-

grams in which an explicit representation of the configurations are stored (i.e., configuration-driven programs), formation of $\mathbf{H}_{P,P}$ and $\mathbf{H}_{Q,P}$ should be quite simple to implement and negligible computationally compared to the cost of the entire calculation. For other schemes, such as integral- or loop-driven methodologies this construction may be more involved, but unless the number of reference configurations is very large and the construction procedure extremely inefficient, the time required to build these matrices should not be prohibitive.

The diagonalization of $\mathbf{H}_{P,P}$ and the transformation of $\mathbf{H}_{Q,P}$ to yield $\mathbf{H}_{Q,\mathrm{MC}}$ are both straightforward matrix operations and should ordinarily require negligible amounts of CPU time (in comparison to the total calculation length). However, for large P spaces in which the entire $\mathbf{H}_{Q,\mathrm{MC}}$ vector is stored on disk this step can become I/O bound. To circumvent this bottleneck $\mathbf{H}_{Q,\mathrm{MC}}$ can be stored in a compressed format in which only the nonzero elements are retained. Since $\mathbf{H}_{Q,P}$ becomes increasingly sparce as the number of reference functions increase the required storage space will be greatly reduced as well as the concomitant I/O difficulties.

The most complicated modification required is the replacement of the diagonalization routine with a procedure to solve a large system of linear equations. Because $\mathbf{H}_{Q,Q}$ cannot be held in core an iterative method in which $\mathbf{H}_{Q,Q}$ is either computed once per iteration or stored on disk must be employed. Most such solvers are based on a method such as the reduced linear equation method proposed by Purvis and Bartlett[34] which has been shown to be a variant of the conjugated gradient method.[35] However, since virtually all large-scale CI programs compute their desired eigenvalues by means of an iterative eigenvalue procedure such as the method of Bartlett and Brandas[36] or Davidson,[37] and since the two types of procedures are computationally very similar, much of the same computer code can be used.

IV. CALCULATIONAL DETAILS FOR F_2

In all calculations performed on F_2 a basis set of better than double zeta plus polarization quality (DZP +) was employed. A modified Huzinaga–Dunning double zeta basis set, originally designated $(9s5p/4s2p)$,[38] was used in which the normal p contraction of 4,1 was changed to 3,1,1, by uncontracting the most diffuse p function while keeping the remaining 3 p exponents unchanged. In addition, a set of six Cartesian d functions with exponent 1.580 were included as polarization functions. We expect that this basis is good enough for meaningful comparisons among the different methods yet is not adequate to describe very accurately dissociation energies and other experimently significant diatomic properties.

The calculations can be divided into three categories: those employing restricted Hartree–Fock (RHF), unrestricted Hartree–Fock (UHF), and multiconfiguration self-consistent field (MCSCF) reference functions. In the one reference RHF and UHF based categories the calculations consist of single reference SCF, CISD, MBPT through full fourth order and CCSD. In addition, the sum of the CCSD plus the fourth order MBPT triples (CCSD + E4T) and CCSDT-1 energies are reported. In all RHF based calculations D_{2h} point group symmetry was used and in the UHF based calculations all spatial orbital symmetry was allowed to break. In all single reference correlated calculations the two 1s core orbitals and their corresponding virtual orbitals were frozen.

The calculations based on the MCSCF reference functions can be subdivided into two groups. In both groups an initial MCSCF optimization is carried out at each geometry followed by subsequent MR-CISD and MR-LCCM calculations. The configuration list for these latter calculations is composed of the MCSCF configurations as reference functions plus the superset of their single and double excitations. These single and double excitations are required to spatially interact directly with the reference space. In addition, where applicable a subset of the spin noninteracting space is removed.[39,40] In the first set of calculations a valence complete active space (CAS) MCSCF consisting of ten reference functions was employed. The second group of calculations are based upon a 32 configuration CAS MCSCF among the $3\sigma_g$, $1\pi_g$, $3\sigma_u$, and $2\pi_u$ orbitals. The first and second sets of calculations will be distinguished via either a -10 or a -32 suffix. The total number of configurations in the MR-10 and MR-32 calculations are 31 334 and 123 018, respectively

In the MR-CISD-10 and MR-LCCM-10 calculations the two 1s core orbitals and their complementary virtual orbitals were frozen. Freezing these virtual orbitals, however, introduces a degree of arbitrariness into the results. Initially, the orbitals generated in the MCSCF procedure were believed to be canonical. However, after completion of the MR-CISD and MR-LCCM curves we discovered that only the core and active orbitals were canonicalized. Several additional MR-CISD calculations were performed in which just the core was frozen and these results show that deleting these virtual orbitals has little effect on the shape of the curve. In the MR-CISD-32 and MR-LCCM-32 calculations only the core was frozen, so this arbitrariness does not exist.

One additional problem occurred initially in the MR-CISD-10 and MR-LCCM-10 calculations. Though the MCSCF-10 curve yielded a 0.04 eV barrier in the region centered at about 6 bohr (similar nonphysical barriers were previously seen by Jonsson *et al.*[3] and Blomberg and Siegbahn[41] in various MCSCF calculations on F_2) the MR-CISD-10 and MR-LCCM-10 results both yielded a steep, roughly 1 eV hump at about 5.8 bohr. This puzzling result was later discovered to have been due to freezing the 1s MCSCF orbitals in the subsequent MR calculations. Since we employed a valence space CAS as our configuration space in the MCSCF and there is only a single vacancy in the F atom valence shell the correlation energy goes to zero in the limit of F_2 separation as a consequence of Brillouin's theorem.[42] Therefore, at some intermediate distance (in our case after about 5 bohr) the occupation of the lowest lying active orbital (the a_1 $2s + 2s$ orbital in D_{2h} symmetry) will become essentially 2 and the energy dependent rotation coupling this orbital with the $1s + 1s$ core will become nearly redundant. What this implies is that massive mixing between

the 1*s* and 2*s* orbitals will cause only a minor change in the MCSCF energy. However, if one of these orbitals is frozen in the later MR calculations and the other is not, the MR energy will change radically in this region as the molecule is separated. To remedy this situation the rotation among these a_1 orbitals was not optimized for F_2 distances beyond 5 bohr. The resulting MCSCF energies were then identical with the original MCSCF energies to all reported figures.

For the RHF based calculations a preliminary set of geometries was chosen to represent the F_2 potential surface from 2.0 bohr to complete dissociation. These geometries and energies are displayed in Table I. For the MCSCF-10, MR-CISD-10, MR-LCCM-10, and MCSCF-32 calculations this same grid was also employed. The MR-CISD-32 and MR-LCCM-32 calculations, however, were each performed at only four geometries, three to describe the minimum and one at large *r* to yield the dissociation energy. These results are displayed in Table II. Only six geometries were considered for the UHF based calculations (except CCSDT-1 for which only the infinitely separated result was computed) since for internuclear distances less than about 2.7 bohr the RHF and UHF SCF results were nearly identical. Fewer energies were also computed along the remainder of the curve since we are primarily interested in the general shape of the UHF curves. The UHF geometries and energies are listed in Table III.

Since full CI results are not available in this basis set we decided to use our predicted diatomic curves to compute various spectroscopic properties and compare with experiment, although the modest basis set size prohibits any definitiveness. After the initial RHF and MCSCF based curves were obtained a number of additional geometries were selected for each method to better represent the minimum region and the entire PES as a whole. These supplemental geometries were in general unique to each method since the predicted equilibrium distances varied substantially from curve to curve. While these extra calculations were used to compute the spectroscopic properties listed in Tables IV and V, the individual internuclear distances and energies will not be reported.

A Taylor's series expansion about r_e was least-squares fit to the final sets of energies obtained for each RHF and MR based method and the harmonic vibrational frequency ω_e, the anharmonicity $\omega_e x_e$, the rotational constant B_e, the rovibronic coupling constant α_e, and the centrifugal distortion $\overline{D}_e$ were obtained via second order perturbation theory.[43] For all F_2 curves ten terms were retained in the Taylor's series with the exception of the CCSDT-1 curve which was approximated using an eight-term series instead. The dissociation energies were not taken from this fit, but were deduced directly from the computed energies. The dissociation energy was taken as the difference between the 100 bohr

TABLE I. Selected RHF F_2 energies as a function of internuclear separation for various single-reference methods.[a]

r(F–F)	SCF	MBPT(2)	MBPT(3)	SDQ-MBPT(4)	SDTQ-MBPT(4)
2.0	− 198.597 31	− 198.994 68	− 198.997 13	− 199.001 04	− 199.008 62
2.2	− 198.696 60	− 199.105 18	− 199.105 81	− 199.111 00	− 199.120 03
2.4	− 198.733 11	− 199.154 13	− 199.152 61	− 199.159 45	− 199.170 24
2.5	− 198.737 43	− 199.164 94	− 199.162 34	− 199.170 11	− 199.181 89
2.6	− 198.735 72	− 199.169 81	− 199.166 19	− 199.174 96	− 199.187 77
2.7	− 198.729 73	− 199.170 43	− 199.165 88	− 199.175 70	− 199.189 61
2.8	− 198.720 78	− 199.168 08	− 199.162 75	− 199.173 65	− 199.188 71
2.9	− 198.709 85	− 199.163 75	− 199.157 79	− 199.169 79	− 199.186 06
3.0	− 198.697 67	− 199.158 17	− 199.151 77	− 199.164 87	− 199.182 40
3.2	− 198.671 45	− 199.145 29	− 199.138 54	− 199.153 81	− 199.174 06
3.5	− 198.631 57	− 199.126 31	− 199.120 35	− 199.138 54	− 199.163 50
4.0	− 198.571 85	− 199.105 45	− 199.104 34	− 199.125 27	− 199.160 31
5.0	− 198.488 97	− 199.118 67	− 199.142 36	− 199.142 30	− 199.208 93
6.0	− 198.443 28	− 199.187 25	− 199.255 05	− 199.139 73	− 199.255 55
100.0	− 198.344 72	− 207.656 60	− 211.739 16	3736.959 35	3688.537 22
r(F–F)	CCSD	CCSD + E_{4T}	CCSDT-1	CISD	
2.0	− 199.000 67	− 199.008 25	− 199.008 09	− 198.980 20	
2.2	− 199.110 43	− 199.119 46	− 199.119 25	− 199.087 80	
2.4	− 199.156 81	− 199.167 61	− 199.169 19	− 199.133 40	
2.5	− 199.169 12	− 199.180 89	− 199.180 71	− 199.142 44	
2.6	− 199.173 79	− 199.186 60	− 199.186 51	− 199.145 54	
2.7	− 199.174 33	− 199.188 24	− 199.188 29	− 199.144 38	
2.8	− 199.172 06	− 199.187 12	− 199.187 39	− 199.140 27	
2.9	− 199.167 94	− 199.184 21	− 199.184 78	− 199.134 19	
3.0	− 199.162 71	− 199.180 24	− 199.181 18	− 199.126 86	
3.2	− 199.150 77	− 199.171 03	− 199.172 93	− 199.110 36	
3.5	− 199.133 13	− 199.158 09	− 199.161 62	− 199.085 15	
4.0	− 199.110 99	− 199.146 03	− 199.150 36	− 199.049 69	
5.0	− 199.092 21	− 199.158 84	− 199.145 98	− 199.009 90	
6.0	− 199.087 72	− 199.203 54	− 199.146 80	− 198.995 16	
100.0	...	...	...	− 198.980 56	

[a] All energies and distances in a.u.

TABLE II. Selected F_2 energies as a function of internuclear separation for various multireference methods.[a]

r(F–F)	MCSCF-10	MR-CISD-10	MR-LCCM-10	MCSCF-32	MR-CISD-32	MR-CCSD-32
2.0	− 198.628 73	− 198.985 26	− 199.005 89	− 198.671 23	···	···
2.2	− 198.739 33	− 199.096 85	− 199.118 32	− 198.782 88	···	···
2.4	− 198.790 01	− 199.146 95	− 199.168 87	− 198.832 41	···	···
2.5	− 198.802 48	− 199.158 58	− 199.180 56	− 198.843 57	···	···
2.6	− 198.809 57	− 199.164 53	− 199.186 46	− 198.848 95	···	···
2.65	···	···	···	− 198.850 05	− 199.171 94	− 199.190 46
2.7	− 198.812 96	− 199.166 51	− 199.188 32	− 198.850 32	− 199.172 46	− 199.190 54
2.75	···	···	···	− 198.849 93	− 199.172 30	− 199.189 95
2.8	− 198.813 89	− 199.165 84	− 199.187 46	− 198.849 02	···	···
2.9	− 198.813 25	− 199.163 49	− 199.184 90	− 198.846 01	···	···
3.0	− 198.811 68	− 199.160 18	− 199.181 37	− 198.842 04	···	···
3.2	− 198.807 32	− 199.152 47	− 199.173 26	− 198.833 08	···	···
3.5	− 198.800 73	− 199.141 68	− 199.162 10	− 198.820 85	···	···
4.0	− 198.793 55	− 199.130 14	− 199.150 34	− 198.808 18	···	···
5.0	− 198.789 45	− 199.123 91	− 199.144 13	− 198.800 84	···	···
6.0	− 198.789 13	− 199.123 15	− 199.143 38	− 198.799 86	···	···
100.0	− 198.789 30	− 199.121 65	− 199.143 47	− 198.799 48	− 199.125 62	− 199.144 40

[a] For the MR-CISD and MR-LCCM calculations at 5.0 and 6.0 bohr the 1*s*–2*s* orbital rotation was not optmized in the MCSCF. The MCSCF energies are unchanged to the reported accuracy. See the text for details.

and equilibrium energies except in the single reference MBPT/CC cases. In these cases due either to convergence difficulties or to severe divergence of the perturbation series the dissociation energy was estimated as the difference between the equilibrium value and the farthest "reasonable" energy (in most cases 4.0 bohr). Also, for the methods where the 100 bohr UHF result is known a second hybrid dissociation result is reported.

Lastly, the zero-point energies and several of the low lying vibrational frequencies were computed for all RHF and MR based methods via numerical solution of the rovibronic equations. For each set of computed points a much larger set of interpolated points was generated from successive fourth-order polynomial fits to adjacent groups of five points. The small and large r regions were approximated differently via r^{-12} and decaying exponential functions, respectively. Using this interpolated data the Schrödinger equation was numerically solved for the nuclear motion via the Numerov method.[44]

V. RESULTS AND DISCUSSION FOR F_2

Examining first the RHF-SCF, UHF-SCF, and MCSCF-10 PES's both SCF curves are found to be particularly poor. (See Fig. 1.) The RHF dissociation energy is over six times as large as the experimental value of 1.66 eV and the UHF curve is purely repulsive, since F_2 is the classic example of a molecule that would not exist in the UHF approximation. The behavior of the RHF curve is due to the inability of the restricted SCF to separate correctly into two neutral F atoms at dissociation. The UHF wave function, however, does dissociate correctly, but fails to predict any binding. This is because the $3\sigma_u$ orbital, which is essential for a correct qualitative description of the bonding in F_2, is not included in the SCF wave function. The MCSCF-10 wavefunction, which does include this $3\sigma_g^2 \rightarrow 3\sigma_u^2$ configuration, is found to be bound by 0.67 eV. However, the computed minima of the two bound curves are both quite far from the experimental value of 1.412 Å (all experimental parameters cited are taken from Ref. 45). The RHF-SCF and MCSCF-10 values of 1.332 and 1.482 Å, respectively, are both nearly 0.1 Å in error. This suggests that inclusion of the $3\sigma_u$ orbital alone is not sufficient if an accurate equilibrium geometry is required.

Given the poor performance of the RHF-SCF PES, can any ordinary single-reference RHF based correlated method improve the surfaces until the point where their overall shape and dissociation energies are essentially correct? In Fig. 2 the results of the finite order MBPT calculations are plotted along with our best estimate of the full CI curve. As the order in perturbation theory is increased the MBPT series appears to converge to the limiting value in the region up to approximately 3.5 bohr. However, beyond 4 bohr the perturbation series diverges, no doubt due to the near degeneracy of the $3\sigma_g$ and $3\sigma_u$ orbital energies. In fact at 100 bohr

TABLE III. Selected UHF F_2 energies in a.u. as a function of internuclear separation.

r(F–F)	SCF	MBPT(2)	MBPT(3)	SQD-MBPT(4)	SDTQ-MBPT(4)	CCSD	CCSD + E_{4T}
2.7	− 198.743 95	− 199.124 80	− 199.133 18	− 199.145 96	− 199.154 70	− 199.172 70	− 199.181 44
3.0	− 198.763 36	− 199.110 33	− 199.123 59	− 199.131 56	− 199.137 65	− 199.159 32	− 199.165 40
4.0	− 198.792 18	− 199.118 10	− 199.133 98	− 199.137 05	− 199.141 00	− 199.138 57	− 199.142 52
5.0	− 198.795 62	− 199.119 72	− 199.135 79	− 199.138 51	− 199.142 24	− 199.139 15	− 199.142 88
6.0	− 198.796 14	− 199.119 94	− 199.136 03	− 199.138 71	− 199.142 41	− 199.139 32	− 199.143 02
100.0	− 198.796 42	− 199.120 12	− 199.136 22	− 199.138 89	− 199.142 58	− 199.139 50	− 199.143 18

TABLE IV Spectroscopic constants for F_2.

Type of Calculation[a]	R_e[b]	D_e[c]	Taylor expansion fit[d] ω_e	$\omega_e x_e$	β_e	α_e	$\bar{D}_e$
SCF	1.3319	10.688	1254	7.6	1.000	8.6	255
CISD	1.3852	4.491	1050	9.1	0.925	10.3	287
SDQ-MBPT(4)	1.4135	1.376 (1.005)	930	12.1	0.888	12.9	324
CCSD	1.4102	2.362 (0.953)	945	12.6	0.892	12.7	318
SDTQ-MBPT(4)	1.4343	0.798 (1.280)	850	14.4	0.863	14.9	356
CCSD + E_{4T}	1.4300	1.149 (1.226)	870	19.1	0.868	14.9	345
CCSDT-1	1.4338	1.129 (1.219)	844	14.8	0.863	15.9	361
MCSCF-10	1.4824	0.669	653	17.3	0.808	21.1	494
MR-CISD-10	1.4386	1.222	821	15.2	0.858	16.1	375
MR-LCCM-10	1.4350	1.221	842	15.3	0.862	15.7	361
MCSCF-32	1.4256	1.384	871	14.3	0.873	14.9	351
MR-CISD-32	1.436	1.275					
MR-LCCM-32	1.439	1.257					
Experiment[e]	1.412	1.66	917	11.2	0.8902	14.1	330

[a] All calculations are spin restricted.
[b] Equilibrium geometries in angstroms. MR-CISD-10 and MR-LCCM-10 values estimated via parabolic fit.
[c] Dissociation energy in eV. In the SCF, MCSCF, CISD, MR-CISD, and MR-LCCM cases D_e was computed as $R(100\text{ a.u.}) - r_e$. For SDQ-MBPT(4), SDTQ(MBPT), CCSD, and CCSD + E_{4T} the first values are $R(4.0\text{ a.u.}) - r_e$ [except for CCSD and CCSDT-1 which are $R(6.0\text{ a.u.}) - r_e$] while the value in parentheses is the corresponding UHF value at 100 a.u. less the RHF r_e value.
[d] ω_e, $\omega_e x_e$, and β_e in cm^{-1}. α_e and $\bar{D}_e$ are in cm^{-1} scaled by 10^3 and 10^8, respectively.
[e] Reference 45.

the MBPT(4) energy is in error by over 3000 hartree!

How well do the CISD and CCSD methods represent the F_2 potential? Since both are "infinite-order" methods in certain senses (CISD is exact perturbation theory in a SD truncated configuration space while the CCSD energy is determined by a summation of certain MBPT diagrams derived from $\hat{T}_1$ and $\hat{T}_2$ cluster operators and their products to all orders) the PES's are expected to behave better at long range than the finite order results. In addition, due to the variational nature of CI, the CISD curve must lie between the SCF and full CI results. In Fig. 3 the potential curves for CISD and CCSD along with the SCF, CCSDT-1, and the various MR-10 curves are plotted so that the minimum energies of all curves coincide. The CISD dissociation value is found to be 4.5 eV. Though a vast improvement over the RHF-SCF value of 10.7 eV, the CISD well depth is still nearly three times too deep. In contrast the size-extensive CCSD model provides a D_e of 2.4 eV which is only about 40% in error. (Due to convergence difficulties with the CC equations at large internuclear separations caused by the incor-

TABLE V. Zero-point energy and the first five vibrational frequencies obtained via numerical solution of the rovibronic equations for F_2 using several different RHF-based methods.

Type of calculation	$G(0)$[a]	$\Delta G_{1/2}$	$\Delta G_{3/2}$	$\Delta G_{5/2}$	$\Delta G_{7/2}$	$\Delta G_{9/2}$
SCF	625	1239	1224	1209	1194	1180
CISD	523	1032	1014	996	979	961
SDQ-MBPT(4)	462	906	881	857	832	807
CCSD	470	926	910	894	873	848
SDTQ-MBPT(4)	421	820	790	759	727	693
CCSD + E_{4T}	431	843	819	796	772	746
CCSDT-1	418	814	784	753	723	691
MCSCF-10	322	618	583	548	511	477
MCSCF-32	432	842	813	784	754	724
MR-CISD-10	406	790	759	728	698	665
MR-LCCM-10	417	811	780	749	717	685
Experiment	456[b]	894	870	846	821	796

[a] $G(0)$ and the vibrational frequencies are all in cm^{-1} and are for the $J = 0$ rotational state.
[b] The experimental zero-point energy is estimated via $G(0) = 1/2\omega_e - 1/4\omega_e x_e$. ω_e and $\omega_e x_e$ are listed in Table III.

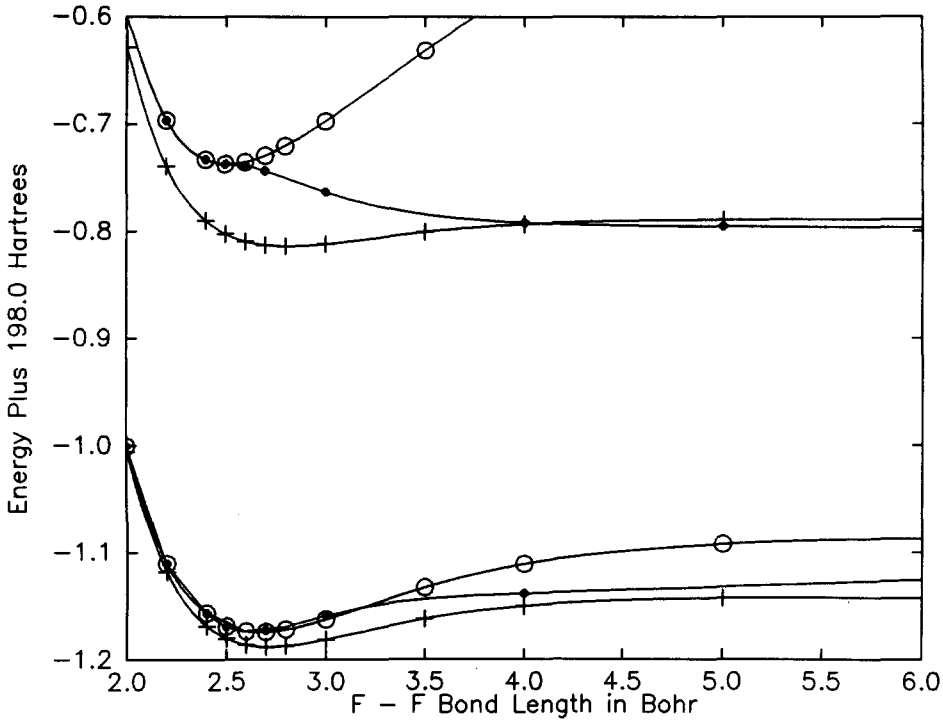

FIG. 1. RHF- and UHF-SCF, MCSCF-10, RHF- and UHF-CCSD, and MR-LCCM-10 potential curves for F_2. The various curves are identified as follows: (O) RHF-SCF; (●) UHF-SCF; (+) MCSCF-10; (O) RHF-CCSD; (●) UHF-CCSD; and (+) MR-LCCM.

rect dissociation of the RHF reference, the CCSD D_e was computed as the difference between the energies computed at 6.0 bohr and r_e.)

Compared to the r_e values predicted by the RHF-SCF and MCSCF-10 calculations both the CISD and CCSD equilibrium geometries are a major improvement. The CISD value of 1.385 Å is within 0.03 Å of experiment while the CCSD value 1.410 Å is nearly identical with experiment. The CCSD geometry would appear to be somewhat fortuitous since the addition of $\hat{T}_3$ effects to the CCSD model as in either the CCSD + E_{4T} or CCSDT-1 methods lengthens the predicted minimum by at least 0.02 Å. Also, we would expect some error due to basis set size. Since the RHF CISD and CCSD methods both require the same order-of-magnitude computation time and the overall shape of the the CCSD curve is superior to that for the CISD PES, of the two, the CCSD method would appear to be the method of choice when dissociating a single bond. Obviously, such a conclusion follows both from CCSD introducing quadruple and higher excitations and its being size extensive.[46] We will

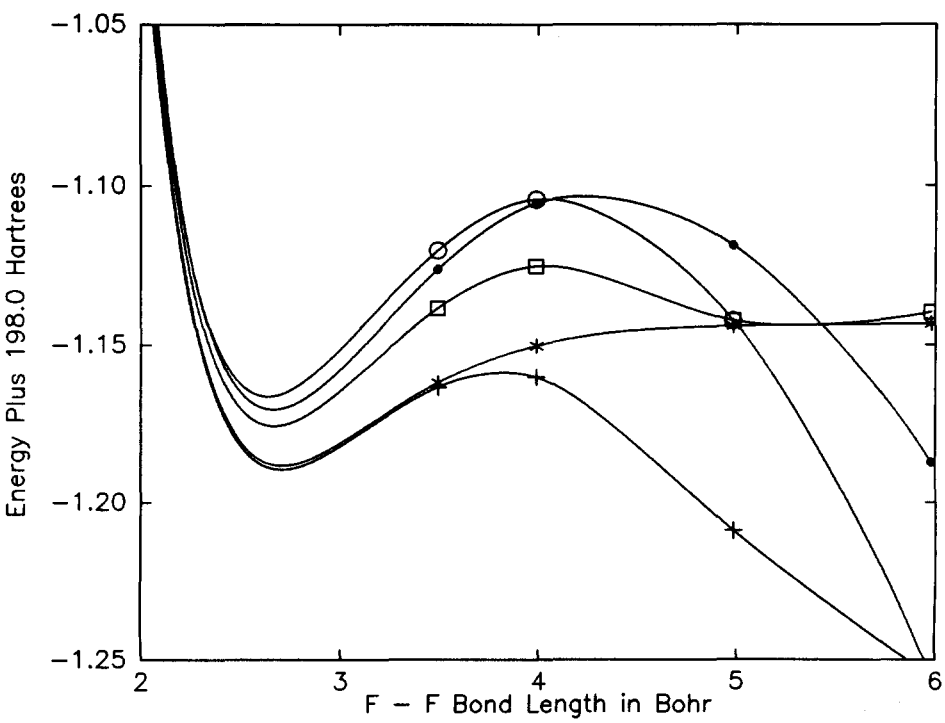

FIG. 2. RHF-based MBPT(2), MBPT(3), SDQ-MBPT(4), MBPT(4), and MR-LCCM-10 potential curves for F_2. The various curves are identified as follows: (O) MBPT(2); (●) MBPT(3); (□) SDQ-MBPT(4); (+) MBPT(4), and (*) MR-LCCM-10.

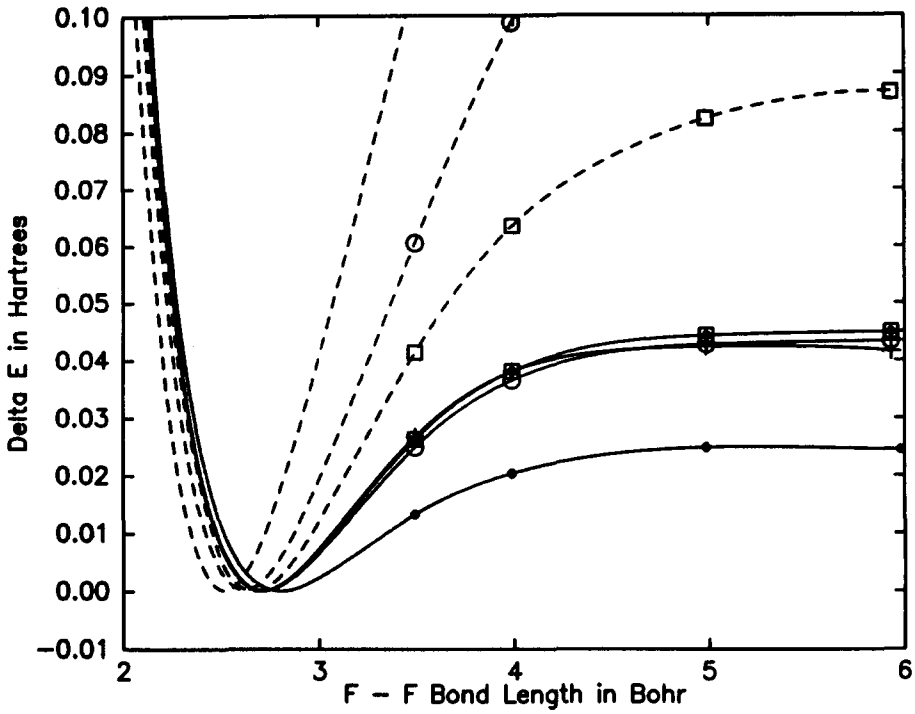

FIG. 3. RHF-based SCF, CISD, CCSD and CCSDT-1, MCSCF-10, MR-CISD-10 and MR-LCCM-10 potential curves for F_2. All potential curves are shifted such that their respective energy minima are zero. The various curves are identified as follows: (– – –) SCF; (○) CISD; (□) CCSD; (+) CCSDT-1; (●) MCSCF-10; (□) MR-CISD-10; and (⊕) MR-LCCM-10.

postpone the discussion on the effects of including triple excitations in RHF-based CC methods (in our case the CCSD + E_{4T} and CCSDT-1 methods) until after the UHF based results have been presented.

In contrast to the RHF methods, the calculations employing the UHF reference function should dissociate to the correct limit, as shown in Fig. 4. This is reflected in the improved D_e values that are obtained by subtracting the RHF-MBPT r_e energy from the corresponding UHF-MBPT energy at dissociation. (The UHF-MBPT energies converge to the RHF-MBPT at r_e.) For MBPT(2) D_e is 1.37 eV and for MBPT(4) the value is 1.28 eV. Both of these values are far superior to the RHF based single-reference CISD and CCSD results. However, since the UHF wave function is not in general an eigenfunction of $\hat{S}^2$ the description of a given spin state can be contaminated by contributions from states of differing spin. For example, the UHF-SCF spin multiplicity at 3.0 bohr is 1.99 nearly twice as large as the pure singlet value. For the ground state of F_2 the multiplicity must approach 1.00 in the full CI limit, however, even at the CCSD level the multiplicity is still only 1.38. The effect of this state mixing is most visible in the so-called recoupling region

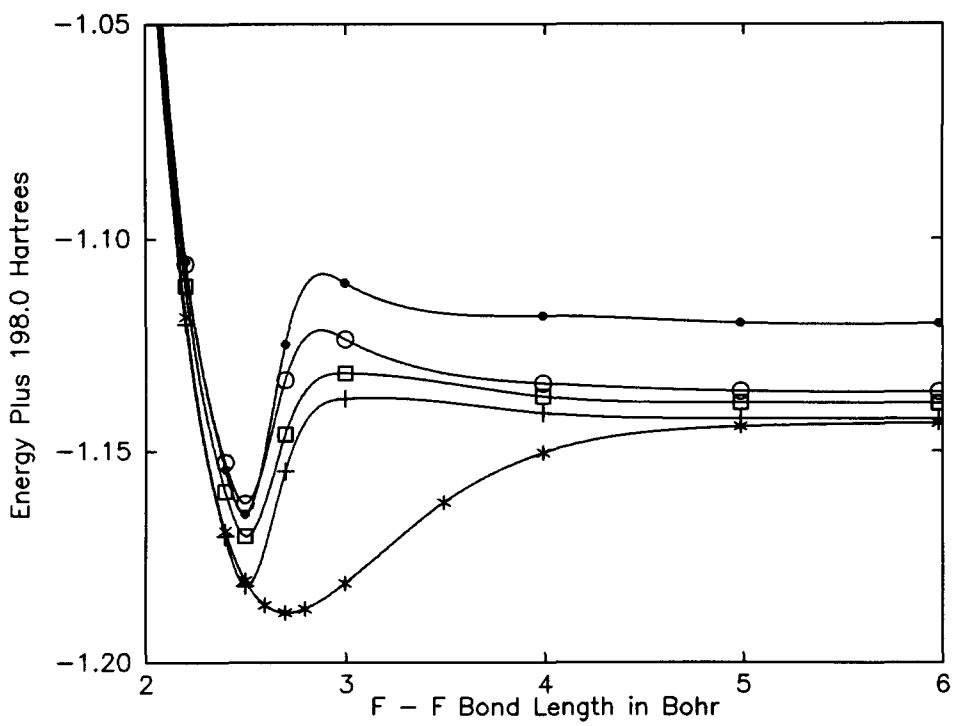

FIG. 4. UHF-based MBPT(2), MBPT(3), SDQ-MBPT(4), and MBPT(4) and MR-LCCM-10 potential curves for F_2. The various curves are identified as follows: (●) MBPT(2); (○) MBPT(3); (□) SDQ-MBPT(4); (+) MBPT(4); and (*) MR-LCCM-10.

which normally occurs at geometries somewhat beyond the equilibrium distance. For example, in all finite order UHF-MBPT calculations performed a nonphysical barrier is observed in the region between 2.8 and 2.9 bohr, as seen in Fig. 4. Due to the limited number of geometry points computed along the UHF curves the barrier height is not known accurately, but it is at least 0.3 eV for MBPT(2) and MBPT(3), and is still over 0.1 eV at MBPT(4). Clearly, spin annihilation of contaminating multiplicities is appropriate for UHF based correlated methods. We have considered spin annihilation as a by-product of monitoring $\hat{S}^2$ in such calculations,[47] and others have implemented such an approach.[48]

Before examining the UHF-CCSD PES and comparing the results with experiment it is important to determine how closely this limit can be approached within this DZP + basis set. Two earlier studies by Jonsson *et al.* (JRTS)[3] and Urban *et al.* (UNK)[49] both employed basis sets similar to the one used presently. When comparable calculations were carried out such as JRTS's two configuration (TC) CISD and our MR-CISD-10 calculations and UNK's and our SDQ-MBPT(4) and MBPT(4) calculations very similar results are obtained. For example, the predicted r_e and D_e obtained by JRTS from their TC-CISD calculations were 1.434 Å and 1.31 eV, respectively. These results are quite close to our values of 1.439 Å and 1.22 eV. Also good agreement is found for ω_e, $\omega_e x_e$ and B_e.

In the best theoretical study of F_2 to date, Siegbahn and Blomberg[41] pointed out two major deficiencies with the earlier calculations of JRTS. First that the configurations $3\sigma_g\ 1\pi_g \rightarrow 3\sigma_u\ 2\pi_u$ are qualitatively important[49] and should be included in the reference space and second, that for accurate geometry predictions *f* functions are required in the basis set. Inclusion of the $3\sigma_g\ 1\pi_g \rightarrow 3\sigma_u\ 2\pi_u$ reference configurations did indeed raise our estimate of D_e from 1.22 to 1.28 eV, however, the equilibrium bond distance only changed by 0.003 Å. Comparing our best calculations for F_2 (RHF-CCSDT-1 at r_e, UHF-CCSDT-1 at D_e, and the various MR-10 and MR-32 calculations at both r_e and D_e) leads us to the conclusion that our basis set limit for r_e is 1.440 ± 0.005 Å and for D_e is 1.26 ± 0.05 eV.

Returning to the discussion of the UHF results the UHF-CCSD curve in contrast to the finite order results does not appear to have a barrier. In fact the only substantial defect in the curve lies in the region between about 2.6 and 3.2 bohr. In Fig. 5 the UHF-CCSD curve can be seen to deviate more than its counterpart RHF PES from the presumably more accurate MR-LCCM curve. This latter PES will henceforth be used as our best estimate to the complete CI result in this basis set. This causes the minimum of the UHF-CCSD curve to shift inwards with respect to the RHF-CCSD curve and lie even further from the basis set limiting value. However, as was the case with the finite order UHF based calculations too few points were computed in the equilibrium region to quantitatively determine the r_e value. Examining the PES as a whole, however, (see Fig. 1) the long range behavior of the UHF-CCSD curve is seen to be far superior to that of the RHF-CCSD PES. In fact, the computed UHF-CCSD D_e of 0.95 eV is only about 0.3 eV below our estimate of the limiting D_e value while the RHF-CCSD value of 2.38 eV is over 1 eV too high.

The addition of triple excitations to CCSD as in either the CCSD + E_{4T} or CCSDT-1 models substantially improves the shape of the PES in the short-range and equilibrium regions.

The RHF-CCSD + E_{4T} curve is quite similar to the RHF-MBPT(4) surface except that it generally lies closer to the MR-LCCM-10 PES out to roughly 3.5 bohr beyond which point both curves rapidly become divergent. The

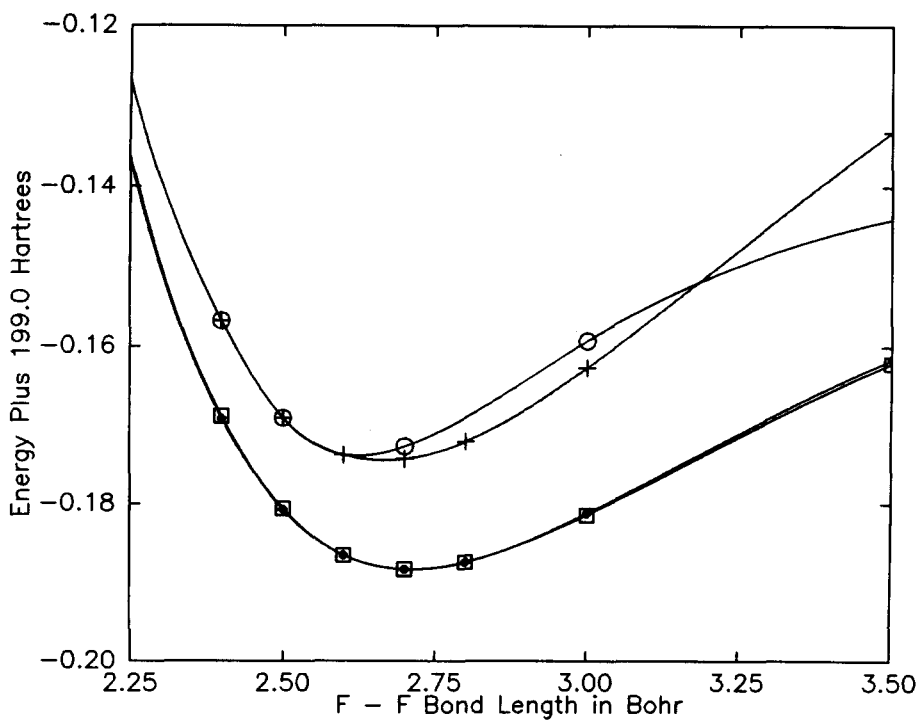

FIG. 5. Closeup view of the equilibrium of the RHF-CCSD, UHF-CCSD, RHF-CCSDT-1, and MR-LCCM-10 potential curves for F_2. The various curves are identified as follows: (+) RHF-CCSD; (○) UHF-CCSD; (●) RHF-CCSDT-1; and (□) MR-LCCM-10.

RHF-CCSDT-1 curve agrees exceptionally well with the MR-LCCM-10 curve from inside the equilibrium region out to around 4 bohr as can be seen in Figs. 3 and 5. Unlike the RHF-MBPT(4) and RHF-CCSD $+ E_{4T}$ curves, however, the CCSDT-1 PES does not become divergent even close to 6.0 bohr (the CCSDT-1 equations would not converge at 100.0 bohr). The slight reduction of the CCSDT-1 curve below the correct separated atom limit shown in Fig. 3 is due to the emerging instability encountered at large internuclear separations. Yet it still yields a respectable dissociation energy of 1.129 eV which is only 0.1 eV lower than the MR-LCCM-10 value. This result suggests that the CCSDT-1 method can correctly separate *single bonds* for most purposes even when an RHF reference is employed.

As is typical of the other single reference methods, moving to the UHF framework can significantly improve the predicted D_e's of the CCSD $+ E_{4T}$ and CCSDT-1 methods. The dissociation energy obtained by subtracting the UHF value for D_e from the RHF value at r_e for CCSD $\pm E_{4T}$ of 1.226 eV is substantially closer to our MR-LCCM (10) result than the analogous MBPT(4) value of 1.280 eV. However, the corresponding CCSDT-1 result of 1.219 eV lies even closer (within 0.002 eV) to the MR-LCCM-10 value (the energy for the UHF-CCSDT-1 100.0 bohr geometry is $-$ 199.143 50 hartree). Unfortunately, we did not compute any additional points on the UHF-CCSDT-1 PES, so there is still a question as to its shape in the recoupling region. In fact, experience suggests that an erroneous curvature due to the remaining spin contamination would still be present in fine detail.[29] However, the quality of the RHF-CCSDT-1 curve and the improvement in the overall shape of the UHF-CCSD PES compared to the RHF-CCSD curve suggests that the UHF-CCSDT-1 surface should be at least reasonable over its entire length.

It is seen from the preceding analysis that none of these RHF and UHF single-reference based methods (at least in the absence of spin projection) can describe all regions of the F_2 PES to high accuracy (with the possible exception of the CCSDT-1 method). In Fig. 3, where various single reference RHF and MR based curves are plotted such that their minimum energies coincide, the MR-CISD-10 and MR-LCCM-10 curves indeed display the qualitatively correct long range behavior and are in fact nearly superimposable upon each other. The D_e for the curves are virtually identical being 1.222 and 1.221 eV for MR-CISD-10 and MR-LCCM-10, respectively. Likewise, the MR-CI and MR-CC equilibrium distances of 1.439 and 1.435 Å, respectively, are quite close. The main qualitative differences between the two curves are in their absolute energies and in the more gradual approach to the dissociation limit energy observed in the MR-CI case. Examining the energy difference first, the MR-LCCM-10 PES is found to lie substantially lower than the MR-CISD-10 surface at all geometries. Similar behavior was observed in previous studies on BeH_2 and H_2O.[1] In fact, in the case of water the MR-LCCM curve was found to be exceedingly close to the full CI value (within 30 μhartree) at a geometry near r_e and to lie only 250 μhartree above the full CI energy at dissociation. Although we would expect the proper MR-CCSD method to be closer to the full CI than a comparable MR-CISD, we attribute this close agreement to some fortuitous error cancellation in the MR-LCCM method, and nonlinear terms must be evaluated to resolve this question. The more gradual approach of the MR-CISD-10 curve to the dissociation energy as F_2 is stretched is visible in Fig. 3. Though the gap between the two shifted MR-10 curves is small it widens to 0.042 eV at 6.0 bohr and then tapers to 0.001 eV at dissociation.

How closely do the MR-10 curves parallel the full CI PES? Earlier, the valence CAS reference space was shown to be qualitatively deficient due to the lack of reference functions involving excitations into the $2\pi_u$ orbital. In Fig. 6 the MCSCF PES's computed using the 10 configuration valence CAS and the larger 32 configuration CAS among the $3\sigma_g$, $1\pi_g$, $3\sigma_u$, and $2\pi_u$ orbitals are plotted. The differences are striking. Comparing the MCSCF-32 to the MCSCF-10 calculations the D_e has been improved by 0.72 eV to 1.38 eV and the equilibrium geometry has been dramatically shortened from 1.482 to 1.426 Å. However, in going from the MR-10 to the equivalent MR-32 calculations D_e and r_e are found in both the CI and CC cases to change only slightly. While the D_e's are improved by 0.05 and 0.04 eV to 1.28 and 1.26 eV in the MR-CISD-32 and MR-LCCM-32 calculations, respectively, the bond lengths change negligibly: 0.001 Å or less in either case. Hence it appears that there are no serious defects in the overall shape of the MR-10 curves at least in the equilibrium and dissociation regions.

Comparison of the absolute energies of the MR-10 and MR-32 curves indicate that, potentially, the MR-LCCM results might be closer in magnitude to the corresponding full CI energies than are the corresponding MR-CISD results. Comparing the energy lowerings obtained by expanding the reference space from 10 to 32 configurations at 2.7 bohr (near equilibrium) the CI lowering is found to be 0.005 95 hartree while the CC value is 0.002 22 hartree. This same lowering at dissociation is 0.003 97 hartree in the CI, but only 0.000 93 hartree in the CC case. The relative stability of the MR-LCCM calculations, with different sized referenced spaces, may be a consequence of their being close to size extensive,[1] unlike the corresponding MR-CI.

Another indication of the accuracy of the MR-LCCM curve is offered through comparison of the best single-reference (SR) calculations and the MR results. Our estimate of the most accurate SR PES (closest in deviation from the full CI surface) are the RHF-CCSDT-1 results in the equilibrium region and the UHF-CCSDT-1 results at dissociation. In the minimum region (2.7 bohr) the RHF-CCSDT-1 result of 199.188 29 hartree is 0.000 03 and 0.002 25 hartree above the CC-10 and CC-32 results, respectively, but is 0.021 78 and 0.015 83 hartree below the CI-10 and CI-32 energies, respectively. A similar trend is visible at dissociation where the UHF-CCSDT-1 energy is within 0.9 mhartree of either MR-LCCM result, but is 17.9 mhartree below the MR-CISD-32 value. In fact, the RHF-CCSDT-1 curve lies within 1 mhartree of the MR-LCCM-10 curve from roughly 2.2 to 4.0 bohr (see Fig. 3).

Examining the spectroscopic constants of the various curves yields another estimate of their quality, at least in the equilibrium region. The inappropriateness of the F_2 RHF-

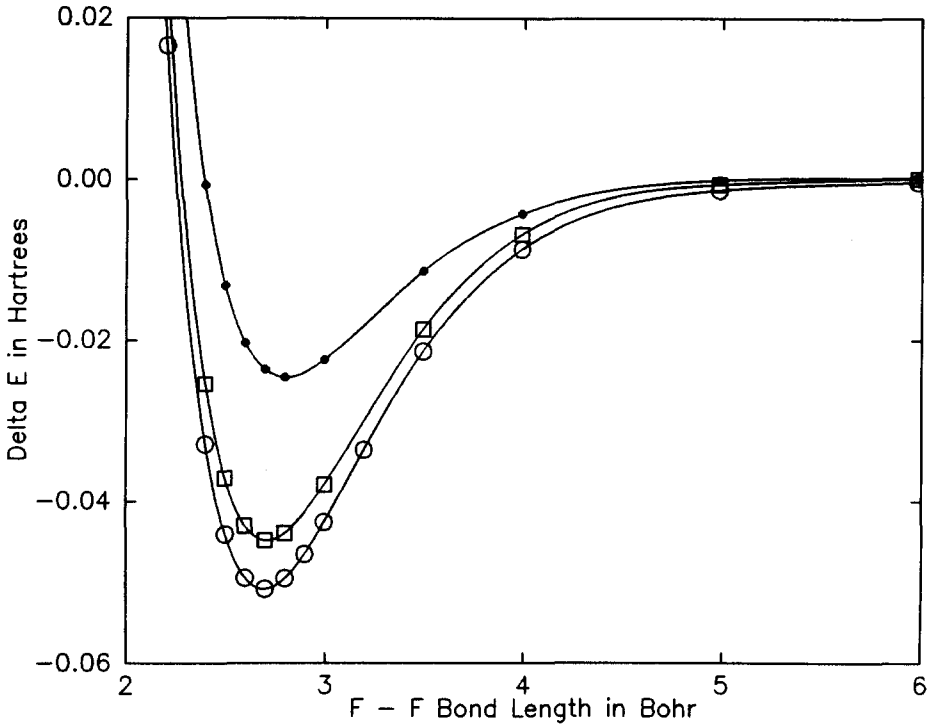

FIG. 6. The MCSCF-10, MCSCF-32, and MR-LCCM-10 potential curves for F_2 shifted such that their respective dissociated energies are zero. The various curves are identified as follows: (●) MCSCF-10; (□) MCSCF-32; and (○) MR-LCCM-10.

SCF surface is clearly reflected in the values for the harmonic frequency ω_e and the first adiabatic frequency $\Delta G_{1/2}$. Ordinarily, SCF frequencies are 10%–20% above the corresponding full CI frequencies, but in this case the error exceeds 40% (assuming that our best calculations are a good estimate to the full CI limit). In addition, the anharmonicity $\omega_e x_e$ is roughly one half of the full CI estimate which implies that the higher adiabatic frequencies will show even poorer agreement.

The importance of including the effect of higher than single and double excitations on the spectroscopic constants is clearly visible in Tables IV and V. The lowest CISD frequency, which is ordinarily within 5% of the full CI value, is still in error by approximately 20% and progressing from the SCF to the CISD model reduces the error in the anharmonicity by only one-fifth. The SDQ-MBPT(4) and CCSD PES's, which take into account most of the quadruple excitation effects in the equilibrium region, yield frequencies that are roughly 10% below the CISD frequencies and anharmonicities which are 30%–40% higher. Most of the remaining discrepancies are alleviated if triple excitations are explicitly included. In the full MBPT(4), CCSD + E_{4T}, and CCSDT-1 calculations the frequencies have again been lowered substantially and the $\omega_e x_e$ values significantly increased. (In fact, the CCSD + E_{4T} $\omega_e x_e$ value of 19.1 cm^{-1} is too high, probably reflecting the mismatch of the infinite and finite order quantities.)

Good agreement is found between the CCSDT-1 constants and those obtained from the MCSCF and MR-10 calculations with the exception of the MCSCF-10 results. As would be expected due to its shallow well depth the MCSCF-10 vibrational frequencies are quite low and $\omega_e x_e$ is too large. On the other hand, the MCSCF-32 frequencies are only marginally larger than the CCSDT-1 values and the two curves have quite similar anharmonicities. Our best complete curves, the MR-CISD-10 and MR-LCCM-10 PES's, both have lower corresponding vibrational frequencies and somewhat higher $\omega_e x_e$ values than in the CCSDT-1 case, though the MR-LCCM-10 and CCSDT-1 harmonic frequencies only differ by 3 cm^{-1}. While there is a larger 21 cm^{-1} difference between either of the MR-CISD-10 harmonic and first adiabatic frequencies and their MR-LCCM-10 counterparts, respectively, the two anharmonicities are within 0.1 cm^{-1}. A similar frequency difference is also visible in the $\Delta G_{1/2} \rightarrow \Delta G_{7/2}$ series, where the CI frequencies are lower than the corresponding CC frequencies by a nearly constant 19 to 21 cm^{-1}. Although perhaps accidentally due to error cancellation, of the two surfaces we consider the MR-LCCM-10 PES to be the most accurate for the reasons presented above and this is supported by its closer proximity to the CCSDT-1 and MCSCF-32 results.

VI. CALCULATION DETAILS FOR N_2

As in F_2 all N_2 calculations employ a modified Huzinaga–Dunning double-zeta (9*s*5*p*/4*s*2*p*) basis set[38] augmented with six Cartesian *d* polarization functions of exponent 0.900.[51] Again the primitive *p* functions are combined to yield three contracted functions instead of the ordinary two in a manner equivalent to that described earlier for F_2. The symbol DZP + will be used to represent this basis set.

The categories and types of calculations performed are equivalent to those detailed previously for F_2. For the RHF and MCSCF based calculations a set of 13 geometries was initially selected to represent the N_2 PES. These geometries are shown explicitly in Table VI. UHF based calculations were also carried out at several of these geometries and are listed in Table VII (for UHF-CCSDT-1 only the dissociated

TABLE VI. Selected RHF N_2 energies as a function of internuclear separation.[a]

r(N–N)	SCF	MBPT(2)	MBPT(3)	SDQ-MBPT(4)	MBPT(4)	CCSD
1.500	– 108.437 26	– 108.700 86	– 108.710 95	– 108.712 74	– 108.720 11	– 108.712 69
1.800	– 108.904 55	– 109.196 82	– 109.200 87	– 109.205 30	– 109.216 76	– 109.204 72
1.900	– 108.951 42	– 109.255 62	– 109.256 05	– 109.262 13	– 109.275 58	– 109.261 15
2.000	– 108.968 01	– 109.285 53	– 109.281 19	– 109.289 56	– 109.305 43	– 109.287 97
2.068	– 108.966 62	– 109.294 03	– 109.285 65	– 109.296 06	– 109.313 85	– 109.293 88
2.500	– 108.835 61	– 109.244 15	– 109.186 66	– 109.228 16	– 109.265 94	– 109.215 04
2.750	– 108.726 23	– 109.197 73	– 109.082 91	– 109.172 56	– 109.230 75	– 109.139 19
3.000	– 108.618 85	– 109.165 47	– 108.960 76	– 109.145 49	– 109.233 17	– 109.067 02
4.000	– 108.289 43	– 109.241 61	– 108.163 54	– 110.004 65	– 110.330 14	– 108.929 26
5.000	– 108.100 00	– 109.576 97	– 106.435 40	– 115.167 96	– 115.943 64	···
6.000	– 107.990 52	– 110.066 05	– 103.302 90	– 130.343 67	– 131.768 45	···
100.000	– 107.698 24	···	···	···	···	···
r(N–N)	CCSD + E_{4T}	CCSDT-1	CISD	MCSCF	MR-CISD	MR-LCCM
1.500	– 108.720 06	– 108.715 98	– 108.700 05	– 108.526 80	– 108.710 80	– 108.718 54
1.800	– 109.216 18	– 109.211 57	– 109.187 94	– 109.022 17	– 109.208 05	– 109.216 63
1.900	– 109.274 60	– 109.269 25	– 109.242 60	– 109.079 99	– 109.266 34	– 109.275 17
2.000	– 109.303 84	– 109.297 66	– 109.267 41	– 109.108 32	– 109.295 16	– 109.304 22
2.068	– 109.311 68	– 109.304 83	– 109.271 82	– 109.115 34	– 109.302 54	– 109.311 76
2.500	– 109.252 82	– 109.236 15	– 109.180 54	– 109.045 36	– 109.235 66	– 109.245 90
2.750	– 109.197 38	– 109.167 96	– 109.095 00	– 108.976 52	– 109.169 31	– 109.180 19
3.000	– 109.154 70	– 109.105 25	– 109.010 92	– 108.913 10	– 109.108 61	– 109.120 20
3.500	– 109.140 07	– 109.027 44	– 108.867 80	– 108.827 49	– 109.026 13	– 109.039 01
4.000	– 109.254 75	– 109.044 83	– 108.761 69	– 108.796 95	– 108.984 77	– 109.005 61
5.000	···	– 109.102 45	– 108.631 23	– 108.789 43	– 108.980 40	– 108.992 85
6.000	···	···	– 108.562 62	– 108.789 03	– 108.978 79	– 108.991 10
100.000	···	···	– 108.421 18	– 108.788 80	– 108.977 86	– 108.990 04

[a] All energies and distances in a.u.

energy was computed and it is specified in Sec. VI). As was the case previously for F_2 all RHF and MCSCF based calculations again employ D_{2h} symmetry and all spatial symmetry was allowed to break in the UHF based computations. Again the 1*s* core and their corresponding virtual orbitals are kept frozen in all correlated calculations (except in the MCSCF procedure itself).

The MR-CISD and MR-LCCM calculations employ a 176 configuration reference space determined from a valence space CAS MCSCF calculation. The complete configuration space in the multireference calculations is composed of the references plus all their single and double excitations yielding a total of 182 656 spin and space adapted interacting configurations.

Spectroscopic properties are computed for the various methods based on least square fits to a Taylor's series expansion about r_e and numerical solution of the rovibronic equations as described previously for F_2. In the course of determining these properties, energies at several additional geometries were also computed for each method to better describe the minimum region. These energies will not be explicitly reported. In the Taylor's expansion eight to nine terms were retained in the series depending on the calculational type. The predicted equilibrium geometries, dissociation energies and Taylor's expansion parameters are displayed in Table VIII and the zero-point energies and lowest vibrational frequencies are collected in Table IX.

VII. RESULTS AND DISCUSSION FOR N_2

Examining the SCF curves first, both the RHF and UHF PES's do a very poor job of describing the ground state of N_2. The RHF-SCF potential well is over three times as deep as the experimental value of 9.91 eV and the equilibrium bond distance is nearly 0.03 Å shorter. Furthermore, for reasons that will soon become apparent we estimate that the full CI limit equilibrium bond distance is actually around 1.113 Å making the SCF agreement even worse. The UHF-

TABLE VII. Selected UHF N_2 energies as a function of internuclear separation.

r(N–N)	SCF	MBPT(2)	MBPT(3)	SDQ-MBPT(4)	SDTQ-MBPT(4)	CCSD	CCSD + E_{4T}
2.25	– 108.933 81	– 109.240 91	– 109.240 31	– 109.259 29	– 109.276 68	– 109.277 19	– 109.294 58
2.5	– 108.882 58	– 109.137 48	– 109.152 76	– 109.169 36	– 109.181 22	– 109.214 07	– 109.225 92
2.75	– 108.837 65	– 109.069 00	– 109.090 03	– 109.102 00	– 109.111 12	– 109.139 81	– 109.148 92
3.0	– 108.802 84	– 109.017 61	– 109.042 53	– 109.052 20	– 109.059 31	– 109.076 94	– 109.084 05
3.5	– 108.779 35	– 108.958 92	– 108.986 61	– 108.993 07	– 108.996 35	– 109.007 25	– 109.010 54
4.0	– 108.784 46	– 108.950 50	– 108.977 72	– 108.982 18	– 108.984 19	– 108.986 62	– 108.988 63
5.0	– 108.793 16	– 108.952 60	– 108.979 44	– 108.983 17	– 108.984 63	– 108.983 93	– 108.985 39
∞	– 108.795 09	– 108.952 88	– 108.979 58	– 108.983 23	– 108.984 57	– 108.983 77	– 108.985 11

TABLE VIII. Spectroscopic constants for N_2.[a]

Type of calculation	r_e[b]	D_e[c]	Taylor expansion fit[d] ω_e	$\omega_e x_e$	β_e	α_e	$\bar{D}_e$
SCF	1.0703	34.57 (4.719)	2721	10.7	2.102	13.6	502
CISD	1.0958	23.15	2471	11.8	2.005	15.0	528
SDQ-MBPT(4)	1.1075	8.524	2316	16.2	1.963	17.9	564
CCSD	1.1037	8.445	2384	12.8	1.977	15.9	544
SDTQ-MBPT(4)	1.1205	9.022	2148	21.9	1.918	21.9	611
CCSD + E_{4T}	1.1156	8.935	2232	16.6	1.934	18.8	581
CCSDT-1	1.1110	8.703	2304	13.3	1.951	16.5	559
MCSCF	1.1098	8.903	2319	13.8	1.955	16.7	556
MR-CISD	1.1120	8.857	2296	14.1	1.947	17.1	560
MR-LCCM	1.1128	8.778	2288	14.2	1.944	17.2	561
Experiment[e]	1.0977	9.91	2359	14.3	1.998	17.3	576

[a] All calculations are spin restricted.
[b] Equilibrium geometries in angstroms.
[c] Dissociation energy in eV. In the SCF, MCSCF, CISD, MR-CISD, and MR-LCCM cases D_e was computed as $E(100 \text{ a.u.}) - E(r_e)$, while the UHF result is in ( ). For SDQ-MBPT(4), SDTQ(MBPT), and CCSD + E_{4T} the perturbation theory is divergent, so these values are obtained from the UHF-CC/MBPT energy at infinite separation less the RHF-CC/MBPT r_e value.
[d] ω_e, $\omega_e x_e$, and β_e in cm^{-1}. α_e and $\bar{D}_e$ are in cm^{-1} scaled by 10^3 and 10^8, respectively.
[e] Reference 45.

SCF curve, on the other hand, is far too shallow. The UHF D_e is only 4.72 eV, which is less than half the experimental value. In addition, the UHF wave function is highly spin contaminated (e.g., the multiplicity at 2.25 bohr is 1.63) and as a consequence a barrier of at least 0.43 eV is found in the spin recoupling region. Unlike F_2 the bifurcation point between the RHF and UHF curves is at a distance larger than equilibrium and, therefore, the r_e values for the RHF and UHF based methods are identical.

From the finite-order RHF-MBPT calculations the perturbation series is found to diverge beyond approximately 3.0 bohr. Even in the vicinity of the minimum the series is oscillatory and appears to be more slowly convergent than is the norm within equilibrium regions. This is reflected in the values of the predicted equilibrium distances for the various truncations of the MBPT series. The predicted r_e values for MBPT(2), MBPT(3), and MBPT(4) are 1.121, 1.096, and 1.121 Å. In contrast to F_2 where MBPT(4) gave an excellent value for r_e the corresponding value for N_2 is much less certain and due to the oscillatory behavior of the above numbers, one suspects that the true equilibrium distance lies somewhat inside of this value. If the UHF reference function is employed in the MBPT expansion beyond the bifurcation point (about 2.2 bohr) the perturbation series is convergent and nonoscillatory out to the dissociation limit. Overall, the shapes of the various MBPT curves are qualitatively correct, but rise too rapidly beyond the equilibrium region (see Fig. 7) even showing an erroneous curvature as discussed previously.[29(b)] Also, in the MBPT(2), MBPT(3), and SDQ-MBPT(4) PES's small nonphysical barriers are still ob-

TABLE IX. Zero-point energy and first five vibrational frequencies obtained via numerical solution of the rovibronic equations for N_2 using several different RHF-based methods.

Type of calculation	$G(0)$[a]	$\Delta G_{1/2}$	$\Delta G_{3/2}$	$\Delta G_{5/2}$	$\Delta G_{7/2}$	$\Delta G_{9/2}$
SCF	1358	2700	2678	2657	2636	2615
CISD	1233	2447	2423	2400	2377	2353
SDQ-MBPT(4)	1157	2282	2243	2210	2179	2141
CCSD	1189	2358	2331	2304	2279	2255
CCSDT-1	1148	2276	2248	2219	2194	2168
SDTQ-MBPT(4)	1068	2104	2058	2008	1953	1892
CCSD + E_{4T}	1111	2197	2162	2127	2094	2059
MCSCF	1156	2291	2262	2234	2207	2181
MR-CISD	1149	2267	2232	2207	2179	2153
MR-LCCM	1140	2258	2228	2198	2172	2145
Experiment	1176[b]	2330	2301	2273		

[a] $G(0)$ and the vibrational frequencies are all in cm^{-1} and are for the $J = 0$ rotational state.
[b] The experimental zero-point energy was computed via $G(0) = 1/2\omega_e - 1/4\omega_e x_e$ and ω_e and $\omega_e x_e$ are listed in Table III.

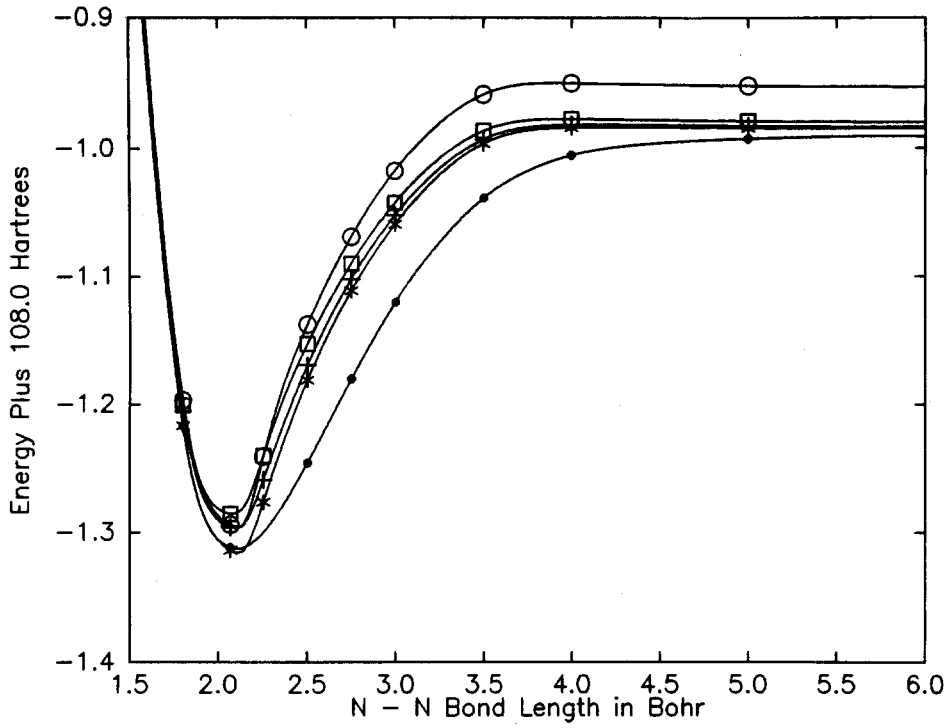

FIG. 7. The UHF-based MBPT(2), MBPT(3), SDQ-MBPT(4), and MBPT(4) and MR-LCCM-10 potential curves for N_2. The various curves are identified as follows: (○) MBPT(2); (□) MBPT(3); (+) SDQ-MBPT(4); (*) MBPT(4); and (●) MR-LCCM.

tained. In MBPT(4) no barrier is found, but there is a very shallow nonphysical second minimum between 4 bohr and dissociation that is roughly 0.02 eV deep (see Table VII).

Do the single-reference RHF-CISD, RHF-, and UHF-CCSD and RHF-CCSDT-1 PES's overcome the deficiencies found in the SCF and MBPT treatments? In Fig. 8 the CISD results are plotted along with the results of the various other RHF and MCSCF based calculations. The CISD surface offers only a modest improvement over the RHF-SCF PES. Though the CISD D_e is over 11 eV lower than the RHF-SCF D_e value the CISD dissociation energy is still too high by over a factor of 2 compared to experiment. At first glance the CISD r_e result appears to be a substantial improvement over the methods considered so far since the CISD and experimental r_e values differ by only 0.002 Å. However, from examination of our best calculations a more realistic estimate of the limiting value of r_e in this basis set is 1.113 Å. If this is the case the CISD geometry is still nearly 0.02 Å too short.

The RHF-CCSD calculations, on the other hand, appear to give a much better estimate of the actual r_e within

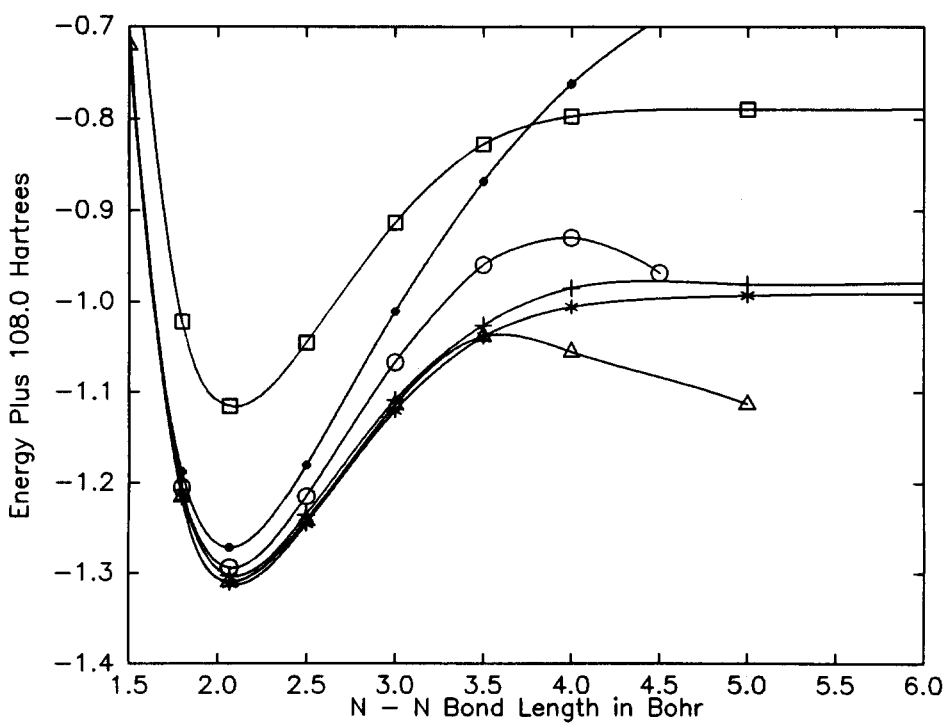

FIG. 8. The RHF-based CISD, CCSD and CCSDT-1, MCSCF, MR-CISD, and MR-LCCM potential curves for N_2. The various curves are identified as follows: (●) CISD; (○) CCSD; (△) CCSDT-1; (□) MCSCF; (+) MR-CISD; and (*) MR-LCCM.

this basis set. The equilibrium bond distance is 0.008 Å longer than in the CISD case, which is roughly half of the remaining error in the geometry. Also, the RHF-CCSD curve is surprisingly accurate out to about 4.0 bohr especially when compared to the RHF-MBPT(4) surface. The RHF-CCSD PES along with the UHF-CCSD and MR-LCCM curves are displayed in Fig. 9. If the dissociation energy is computed as the difference between the minimum and 4.0 bohr energies a value of 9.93 eV is obtained which is over 1 eV above our best estimate of the limiting D_e in this basis. However, as is visible from the figure, there is a nonphysical hump in the RHF-CCSD curve, forced by the incorrect dissociation of the RHF function. Unfortunately, convergence difficulties in the CC equations prohibit us from extending the RHF-CCSD curve beyond 4.5 bohr so whether the RHF-CCSD curve can dissociate to the correct limit remains unanswered.

By comparison the UHF-CCSD curve in Fig. 8 appears to behave at least qualitatively correct along its entire length, and, in particular, largely corrects the UHF + MBPT curves of Fig. 7. Assuming the MR-CISD and MR-LCCM surface are reasonable estimates to the full CI potential the only qualitative defect in the shape of the UHF-CCSD curve visible from the figure is the increased separation of the two curves in the 2.5 to 3.5 region. In fine detail, we might also expect an artificial hump in this region as previously observed for UHF based correlated studies of N_2.[29] These effects are most likely a consequence of spin contamination which is still relatively large in the UHF-CCSD wave function.[29(b)] For example, at 3.0 bohr the multiplicity is 2.22.

The RHF-CCSDT-1 surface in N_2 like its counterpart in F_2 is extremely accurate, virtually paralleling the MR-CI and MR-CC curves from inside the minimum geometry to approximately 3.4 bohr. This might be seen better in Fig. 10 where the minima for the CISD, CCSD, CCSDT-1 and the two multireference curves are superimposed. Beyond about 3.4 a.u., however, the PES rapidly deteriorates and past about 5.0 bohr we were unable to solve the $\hat{T}$ amplitude equations for all geometries. This contrasts to the situation in F_2 where the CCSDT-1 curve behaved correctly out to close to 6.0 bohr. This is most likely a consequence of the high levels of excitation needed to correctly break the N_2 triple bond starting from an RHF reference. A dissociation energy may be estimated if the UHF-CCSDT-1 energy for dissociation (− 108.985 70 hartree) is subtracted from the equilibrium RHF-CCSDT-1 result in computing D_e. This D_e of 8.703 eV is less than 0.1 eV from the MR-LCCM value and should be close to the best basis set result, since for most cases CCSDT-1 agrees with the full CI to within ~1 kcal/mol.[54]

The valence CAS-MCSCF surface, in contrast to the analogous surface in F_2, contains no substantial qualitative defects. This has been pointed out previously by Siegbahn.[52] The quality of the MCSCF surface is apparent in Fig. 11 where the MCSCF, MR-CISD and MR-CCSD curves are plotted so that their energy minima coincide. The r_e value for the MCSCF PES is quite close to both the MR equilibrium distances being only 0.0022 and 0.0030 Å shorter than in the CI cases, respectively. Likewise the MCSCF dissociation energy of 8.903 eV is within 0.125 eV of either MR result. The largest defect visible from the figure is in the region surrounding 3.5 bohr where the MCSCF curve deviates most from either MR surface. As the N_2 bond is stretched from 3.5 bohr to dissociation the MCSCF-MR-LCCM gap narrows by over a factor of 2.

Examining next our two best complete PES's, in Figs. 8,

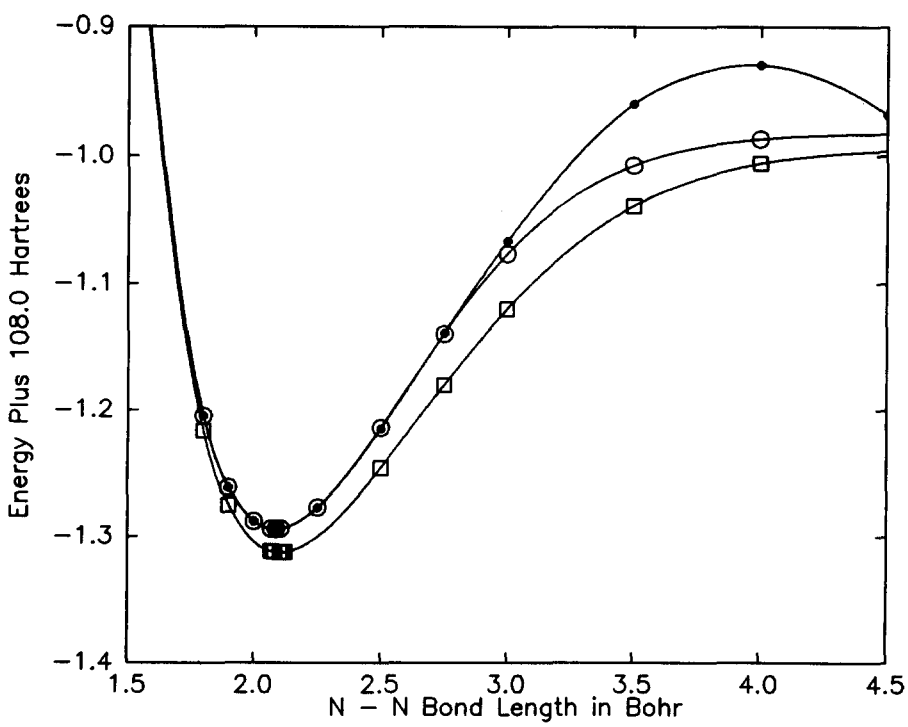

FIG. 9. The RHF-CCSD, UHF-CCSD, and MR-LCCM potential curves for N_2. The various curves are identified as follows: (●) RHF-CCSD; (○) UHF-CCSD; and (□) MR-LCCM.

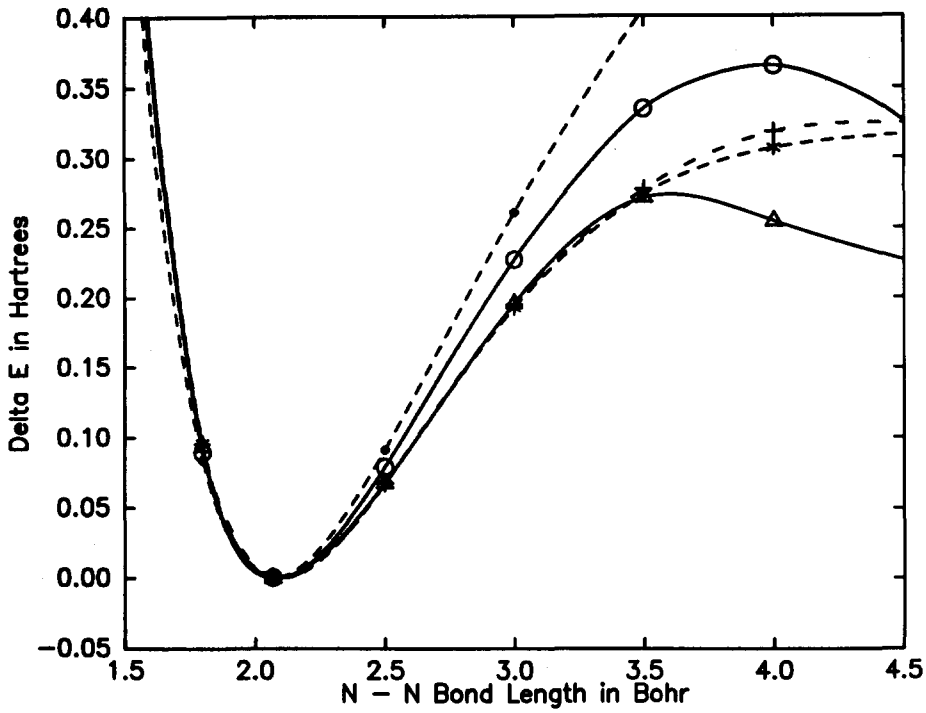

FIG. 10. The RHF based CISD, CCSD, CCSDT-1, and the MR-CISD and MR-LCCM curves for N_2 with their minima superimposed. The various curves are identified as follows: (●) CISD; (○) CCSD; (△) CCSDT-1; (+) MR-CISD; and (*) MR-LCCM.

10, and 11, the MR-CISD and MR-LCCM curves are found to yield very similar values for r_e, 1.1120 and 1.1128 Å, respectively, and are virtually superimposable out to approximately 2.5 bohr. However, beyond this distance the curves are no longer parallel. If the two surfaces are positioned as in Fig. 11 the largest separation is again found near 3.5 bohr. However, in contrast to the MCSCF results, the difference between the curve separations at 3.5 bohr and at dissociation is now just 0.02 eV compared to the analogous difference of 0.28 eV obtained from the MCSCF and MR-LCCM surfaces.

Of the two MR curves, which one does a better job of describing the DZP + full CI PES? Unlike the situation for F_2 the choice of the MR-LCCM potential is somewhat unclear. First, as opposed to F_2 the single reference calculations in the equilibrium region are not as useful in helping to determine which of the two MR r_e values is the most accurate. The equilibrium geometries of the best SR surfaces, MBPT(4), CCSD, CCSD + E_{4T}, and even CCSDT-1, are all farther from either of the MR r_e values than the two MR r_e values are to each other and, in addition, all of these SR methods except possibly CCSDT-1 have significant defects

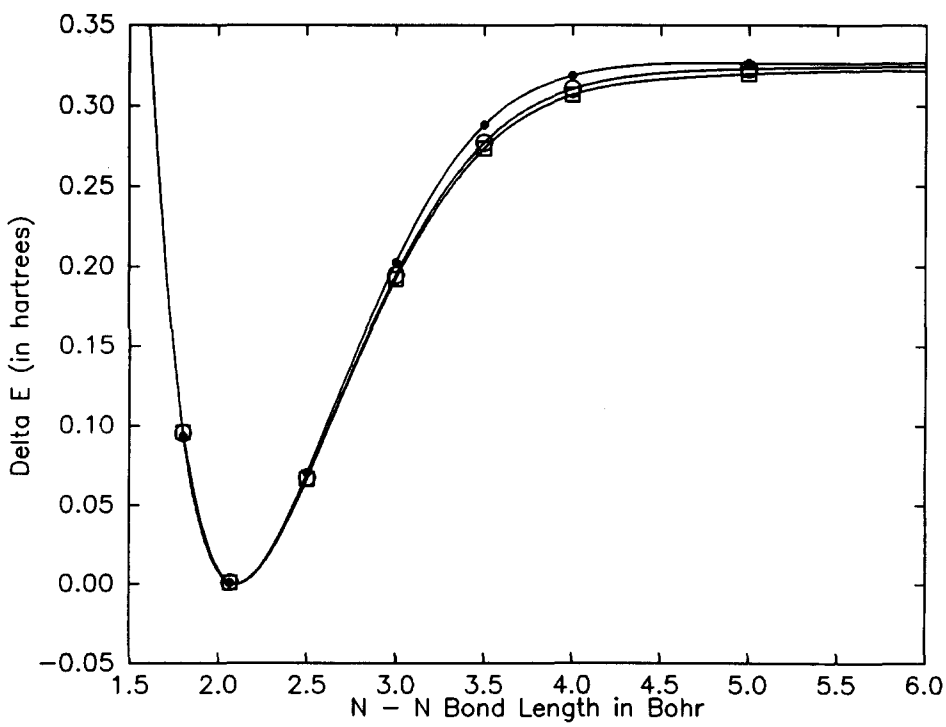

FIG. 11. The MCSCF, MR-CISD, and MR-LCCM potential curves for N_2 shifted such that their respective minimum energies are zero. The various curves are identified as follows: (●) MCSCF; (○) MR-CISD; and (□) MR-LCCM.

in the equilibrium region for this particular case as was pointed out earlier. Second, a similar problem exists for N_2 when comparing the D_e's and the absolute energies. However, the trends observed in the MR N_2 calculations can be compared to those found for the MR calculations in F_2.

In the F_2 MR-32 calculations a relatively minor change in the equilibrium geometry was found between the two curves compared with a more significant change in the dissociation energies. Similar behavior is seen in the N_2 MR calculations. For example, in going from the MR-CISD-32 to MR-LCCM-32 surfaces D_e decreased by 1.4%. In N_2 the analogous D_e lowering is 0.9%. In the smaller MR-10 calculations performed on F_2 there was virtually no change in the dissociation energy. However, as stated earlier the MCSCF-10 reference does a poor job of describing the F_2 potential, so comparison with the MR-32 curves would be more valid.

Around the minimum region the RHF-CCSDT-1 energies are much closer to the corresponding MR-CISD than they are to the corresponding MR-LCCM energies. This is in contrast to the situation in F_2 where the opposite was true. However, at dissociation the UHF-CCSDT-1 energy is closer to the analogous MR-LCCM than the MR-CISD result. Since we no longer have variational results to compare against as we did for F_2 it is impossible for us to know if the MR-LCCM energies have overshot the "exact" results and, consequently, to predict which of the two curves lie closest to the full-CI, but the similar energies obtained by MBPT(4), CCSDT-1, and MR-CISD suggest a likely overestimate of correct binding energy in the MR-LCCM result.

Lastly, the spectroscopic constants obtained from the various RHF PES's will be examined (see Tables VIII and IX). Since the differences between the harmonic frequencies for the various methods are nearly identical with the differences between the "true" first vibrational frequencies ($\Delta G_{1/2}$ values from Table IX) only the trends in ω_e (and $\omega_e x_e$) will be discussed.

Unlike F_2, the SCF and CISD harmonic frequencies for N_2 are typical, lying 15% and 5%, respectively, above the experimental ω_e value of 2359 cm^{-1}. However, as was also the case in F_2, progressing to the CISD level does little to improve the anharmonicity. (In N_2 only 31% of the remaining error in $\omega_e x_e$ relative to experiment is recovered.) The SDQMBPT(4), CCSD, and CCSDT-1 harmonic frequencies are somewhat of an improvement over the CISD result, especially since the full CI value for ω_e in this basis set is probably between 2250 and 2300 cm^{-1}, but MBPT(4) is poorer. The CCSDT-1 anharmonicity is also slightly improved over the CI result, however, the full fourth-order value for $\omega_e x_e$ is nearly twice the experimental value. This is a consequence of the apparent slow rate of convergence of the perturbation series even for the equilibrium region of N_2, and, in particular, the effect of triple excitations as measured by SDTQ-MBPT(4) compared to SDQ-MBPT(4) is seen to move the answer away from experiment. However, once triples are included iteratively as in CCSDT-1, which reduces their net effect as may be measured by comparison to CCSD, agreement is once again achieved. In F_2, where the perturbation series converges much faster, the ω_e and $\omega_e x_e$ values at MBPT(4) are probably close to the "full CI" limiting value. Another indicator of the slow convergence of perturbation theory for N_2 is seen in the large changes between the SDQ-MBPT(4) and the infinite-order sum of such terms as computed by CCSD for $\omega_e x_e$, or by SDTQ-MBPT(4) vs CCSDT-1.

The spectroscopic constants computed using any of the MR PES's (including also the CAS MCSCF PES) appear to be much more accurate than those obtained from any of the single reference approaches that were tried with the exception of CCSDT-1. The quality of the MCSCF reference functions is reflected in the small changes that occur in ω_e and $\omega_e x_e$ in proceeding from the MCSCF to either the MR-CISD or MR-LCCM methods. For example, the difference between the MCSCF and MR-LCCM harmonic frequencies is 31 cm^{-1} compared to the corresponding difference in F_2 between the MCSCF-10 and MC-LCCM-10 ω_e values of 189 cm^{-1}. However, the MCSCF ω_e for F_2 changes by 218 cm^{-1} just be expanding the reference space from 10 to 32 functions. The CCSDT-1 anharmonicity is worse than the MCSCF value (assuming that the MR-CISD and MR-LCCM results are in fact closer to the limiting value), while ω_e is improved, with the other constants negligibly different. The 63 and 71 cm^{-1} discrepancies between the experimental and our MR-CISD and MR-LCCM values for ω_e are most likely due to deficiencies in the basis set, although the potential for errors in the curve fitting procedure cannot be entirely discounted. Siegbahn's study of the N_2 ground and excited states[41] reveals the importance of employing larger than DZP basis sets and including f functions if high accuracy in the N_2 spectroscopic constants is desired. In light of this, the excellent agreement of both the MR-CISD and MR-LCCM anharmonicities with experiment (14.1, 14.2, and 14.3 cm^{-1}, respectively) might be partly fortuitous.

VIII. SUMMARY

A new derivation of the MR-LCCM equations has been presented which is based upon applying the CC ansatz directly to an MCSCF reference function. The MR-LCCM method is designed to compete directly against the traditional MR-CISD procedure and it has been shown how this method can be implemented in an efficient and straightforward manner via modification of existing MR-CI programs. This procedure has been used to investigate the ground-state PES's of F_2 and N_2. Taken as a whole, the MR-LCCM results were shown to compare favorably with those from analogous MR-CISD calculations. For F_2 and N_2 the overall shape of the MR-LCCM PES's (based upon valence-space CAS-MCSCF reference functions) were qualitatively correct and the corresponding MR-CISD curves were nearly superimposible. In both cases, however, the MR-LCCM curves were lower in energy along their entire lengths than the analogous MR-CISD curves. We would hope that this difference is an accurate measure of the difference due to MR-LCCM being nearly size extensive while MR-CISD is not, but further work will have to determine this. In F_2 comparison with the results of the various highly correlated single-reference methods such as MBPT(4), CCSD and especially CCSDT-1 and the larger 32 configuration MR

calculations suggest that the MR-LCCM results lie closer to the "exact" (full-CI) potential than the comparable MR-CISD results, although perhaps fortuitously. For N_2 the situation is less clear cut, but at least in the dissociation region our analysis suggests that the MR-LCCM results are reasonably accurate.

Additionally, it was discovered that the MR-LCCM procedure could overcome a serious qualitative defect in the reference function. For F_2 the valence-space CAS-MCSCF wave function only yields about 50% of our best estimate of the basis set dependent binding energy. However, if the active orbitals are augmented with the $2\pi_u$ orbital the CAS-MCSCF only overestimates this binding energy by roughly 10%. What is surprising is the similarity of the MR-LCCM curves computed employing either of the two MCSCF reference choices; the PES's are shown to be quite close in those regions where both were computed. In addition, the two comparable MR-CISD curves generally show larger discrepancies between themselves than do the two MR-LCCM curves. This suggests that the MR-LCCM method might converge faster to the full-CI limit as a function of increased reference size than does the traditional MR-CISD method, which would be expected for a properly linked-diagram, size extensive method.

One additional very positive result is that the recently proposed single reference CCSDT-1 model[32] has sufficient flexibility that it can largely overcome a very poor RHF single-reference approximation and provide an accurate potential curve far beyond the equilibrium geometry, all the way to dissociation for F_2, and to about $2R_e$ for N_2. In the latter case a UHF-CCSDT-1 result for the atoms is necessary to obtain a reasonable dissociation energy. The comparative simplicity of single-reference methods, and necessity of using such methods in extended systems, recommends the continued extensions of the single-reference theory to include more of T_3 and part of T_4. At that level, it would appear that the approach to the full CI might be sufficiently close that such a method will suffice except for the most difficult cases. However, when nondynamical correlation is very important as in the bond breaking of N_2, some single but multiconfigurational reference CC approach should be quite powerful.

ACKNOWLEDGMENTS

The authors would like to thank Professor Walter C. Ermler for providing the diatomic fitting and vibrational programs that were used to compute the spectroscopic constants cited within; Dr. Ron Shepard for helpful advice concerning degenerate orbital rotations in MCSCF wave functions and for allowing us to use his MCSCF program; Professor Henry F. Schaefer III for allowing us to use and modify his group's unitary group CI code; and to Dr. Samuel J. Cole for computational assistance and many helpful discussions. This research was supported by the U. S. Office of Naval Research.

APPENDIX

In proceeding from Eq. (17) to Eq. (18) we neglect the the term $\mathbf{T}_{Q,Q}\mathbf{H}_{Q,\mathrm{MC}}$; in this Appendix some justification is presented.

A given element in the column vector $\mathbf{T}_{Q,Q}\mathbf{H}_{Q,\mathrm{MC}}$ can be expressed as [see Eq. (16)]

$$\sum_{\Phi_u \in Q} \langle \Phi_r | \hat{T} | \Phi_u \rangle \langle \Phi_u | \hat{H} | \Psi_{\mathrm{MC}} \rangle, \tag{A1}$$

where the functions Φ_u, $u = 1, n_Q$ are a set of orthonormal configurations that span the single and double excitation space relative to the MCSCF reference functions and n_Q is the number of linearly independent functions required to span this space. For reasons that will become apparent later, it is useful to replace the Q space projection operator above $(\Sigma |\Phi_u\rangle\langle\Phi_u|)$ with an alternate Q space projector over the nonorthonormal functions ϕ, where the functions $\phi_v \in Q$ are the set of all functions formed by acting with $\alpha^+ r$, $\alpha^+ r\beta^+ s$, $\alpha^+ r\beta^+ s\gamma^+ t$, etc., upon Ψ_{MC} where the creation and annihilation operators are defined following Eq. (6) with the restriction that all completely internal excitations are excluded. This restriction is a consequence of the P and Q space partitioning. Using this definition of Q then,

$$\sum_{\Phi_u \in Q} \langle \Phi_r | \hat{T} | \Phi_u \rangle \langle \Phi_u | \hat{H} | \Psi_{\mathrm{MC}} \rangle = \sum_{\phi_v, \phi_w \in Q} \langle \Phi_r | \hat{T} | \phi_v \rangle \mathbf{S}^{-1}_{vw} \langle \phi_w | \hat{H} | \Psi_{\mathrm{MC}} \rangle, \tag{A2}$$

where $\mathbf{S}^{-1}_{vw}$ is the inverse of the ϕ-basis overlap matrix.

Next, partition the sets of Φ and ϕ functions into singly and doubly excited subsets (also triply, quadruply, etc., excited subsets in the latter case) and label these sets with the lowercase letters s, d, t, q, etc. To distinquish the Φ from the ϕ functions a prime will be added to the subsets formed from the ϕ functions (s', d', etc.). In determining the excitation class of a particular Φ and ϕ function rearrangement among the active electrons is not considered to constitute an additional excitation. We also introduce a classification scheme that groups elements of the various excitation categories and the individual elements in $\hat{T}$ into several subcategories. Each subcategory will be identified via an ordered pair (i,j) where i represents the decrease in the number of core electrons and j represents the increase in the number of virtual electrons relative to either the SCF or MCSCF vacuum. [The SCF and the MCSCF reference configurations are in the subcategory (0,0).] These two numbers uniquely determine the number of electrons in each of the three categories: core, active, and virtual. The terms in $\hat{T}$ and the excitation classes s, s', d and d' break down into the following subcategories:

Subcategory number	s, s'	d, d'	$\hat{T}$
1	(0,1)		(0,1)
2	(1,0)		(1,0)
3	(1,1)		(1,1)
4		(0,2)	(0,2)
5		(2,0)	(2,0)
6		(2,2)	(2,2)
7		(2,1)	(2,1)
8		(1,2)	(1,2)

The s' and d' submatrix of the $\mathbf{S}^{-1}_{vw}$ matrix can be expressed in terms of these excitation classes as

$$
\begin{array}{c|c|ccc|ccccc}
 & & s' & & & d' & & & & \\
\hline
s' & \langle 1|1\rangle & 0 & 0 & 0 & 0 & 0 & 0 & 0 \\
 & 0 & \langle 2|2\rangle & 0 & 0 & 0 & 0 & 0 & 0 \\
 & 0 & 0 & \langle 3|3\rangle & 0 & 0 & 0 & 0 & 0 \\
\hline
 & 0 & 0 & 0 & \langle 4|4\rangle & 0 & 0 & 0 & 0 \\
 & 0 & 0 & 0 & 0 & \langle 5|5\rangle & 0 & 0 & 0 \\
d' & 0 & 0 & 0 & 0 & 0 & \langle 6|6\rangle & 0 & 0 \\
 & 0 & 0 & 0 & 0 & 0 & 0 & \langle 7|7\rangle & 0 \\
 & 0 & 0 & 0 & 0 & 0 & 0 & 0 & \langle 8|8\rangle
\end{array}
\qquad \text{(A3)}
$$

where, e. g., $\langle 1|1\rangle$ is the inverse overlap matrix between all functions in the (0,1) space. The t' and higher excitations would also breakdown into diagonal blocks, but these terms will not contribute to $\mathbf{T}_{Q,Q}\mathbf{H}_{Q,\mathrm{MC}}$ since terms like $\langle t'|\hat{H}|\Psi_{\mathrm{MC}}\rangle$ are zero because all functions in t' differ by more than two excitations from Ψ_{MC}.

Exploiting the s' and d' block structure of Eq. (A3), Eq. (A2) can be rewritten as

$$
\mathbf{T}_{Q,Q}\mathbf{H}_{Q,\mathrm{MC}} = \begin{bmatrix} \langle s|\hat{T}|s'\rangle\langle s'|s'\rangle^{-1}\langle s'|\hat{H}|\Psi_{\mathrm{MC}}\rangle + \langle s|\hat{T}|d'\rangle\langle d'|d'\rangle^{-1}\langle d'|\hat{H}|\Psi_{\mathrm{MC}}\rangle \\ \langle d|\hat{T}|s'\rangle\langle s'|s'\rangle^{-1}\langle s'|\hat{H}|\Psi_{\mathrm{MC}}\rangle + \langle d|\hat{T}|d'\rangle\langle d'|d'\rangle^{-1}\langle d'|\hat{H}|\Psi_{\mathrm{MC}}\rangle \end{bmatrix}. \qquad \text{(A4)}
$$

Employing the generalized Brillouin theorem (GBT),[53] which states that $\langle\Psi_{\mathrm{MC}}|\hat{H}|(i^+j - j^+i)\Psi_{\mathrm{MC}}\rangle = 0$ for $i<j$, all matrix elements of the type $\langle s'|\hat{H}|\Psi_{\mathrm{MC}}\rangle$ involving "true" single excitations can be shown to be zero. By true we mean the single excitation subset of s' that does not include any active to active excitations. This is because the Q space for this subset does not include any terms involving only all internal excitations and these terms are the only ones for which both the $i^+j|\Psi_{\mathrm{MC}}\rangle$ and $j^+i|\Psi_{\mathrm{MC}}\rangle$ functions exist. In all the other cases at most one of these two functions is nonzero and, therefore, by the GBT the remaining must be equal to zero.

To estimate the magnitude of the remaining terms in Eq. (A4) we next expand the cluster operator matrix elements into sets of matrix elements over the various subcategories. The only nonzero combinations are

$$
\begin{aligned}
&\langle s|\hat{T}|s'\rangle = \{\langle 3|1|2\rangle,\ \langle 3|2|1\rangle\},\\
&\langle s|\hat{T}|d'\rangle = \mathbf{0},\\
&\langle d|\hat{T}|s'\rangle = \{\langle 4|1|1\rangle,\ \langle 5|2|2\rangle,\ \langle 6|3|3\rangle,\ \langle 7|2|3\rangle,\\
&\qquad\qquad \langle 7|3|2\rangle,\ \langle 8|1|3\rangle,\ \langle 8|3|1\rangle,\ \langle 7|5|1\rangle,\\
&\qquad\qquad \langle 8|4|2\rangle,\ \langle 6|7|1\rangle,\ \langle 6|8|2\rangle\},\\
&\langle d|\hat{T}|d'\rangle = \{\langle 7|1|5\rangle,\ \langle 8|2|4\rangle,\ \langle 6|1|7\rangle,\ \langle 6|2|8\rangle,\\
&\qquad\qquad \langle 6|4|5\rangle,\ \langle 6|5|4\rangle\},
\end{aligned}
$$

where the integers in the matrix elements on the right-hand side of the equalities above label the particular subcategories involved. For example, the term $\langle 3|1|2\rangle$ represents the $\langle s|\hat{T}|s'\rangle$ class of matrix elements between the s subcategory (1,1), the $\hat{T}$ subcategory (0,1), and the s' subcategory (1,0).

Combining the individual matrix element expressions above into nonzero terms in the $\mathbf{T}_{Q,Q}\mathbf{H}_{Q,\mathrm{MC}}$ matrix element summation, the $\langle d|\hat{T}|d'\rangle\langle d'|d'\rangle^{-1}\langle d'|\hat{H}|\Psi_{\mathrm{MC}}\rangle$ term is the only one which is not zero when semi-internal excitations are excluded. We argue that since we are employing an MCSCF wave function as our reference function all terms involving semi-internal excitations will be small. This is because the effect of including semi-internal excitations is relaxation within the active space and since the active space configuration coefficients (along with all the orbitals) have already been optimized the subsequent change should be rather small, especially as the size of the MCSCF configuration space increases. (Similar arguments have been used previously by others to justify the complete omission of semi-internal excitations from another multireference CC method.[17]) Neglecting the terms involving semi-internal excitations, then, Eq. (A4) simplifies to

$$
\mathbf{T}_{Q,Q}\mathbf{H}_{Q,\mathrm{MC}} = \begin{bmatrix} \mathbf{0} \\ \langle 6|1|7\rangle\langle 7|7\rangle^{-1}\langle 7|\hat{H}|\Psi_{\mathrm{MC}}\rangle \\ \quad + \langle 6|2|8\rangle\langle 8|8\rangle^{-1}\langle 8|\hat{H}|\Psi_{\mathrm{MC}}\rangle \\ \quad + \langle 6|4|5\rangle\langle 5|5\rangle^{-1}\langle 5|\hat{H}|\Psi_{\mathrm{MC}}\rangle \\ \quad + \langle 6|5|4\rangle\langle 4|4\rangle^{-1}\langle 4|\hat{H}|\Psi_{\mathrm{MC}}\rangle \\ \langle 7|1|5\rangle\langle 5|5\rangle^{-1}\langle 5|\hat{H}|\Psi_{\mathrm{MC}}\rangle \\ \langle 8|2|4\rangle\langle 4|4\rangle^{-1}\langle 4|\hat{H}|\Psi_{\mathrm{MC}}\rangle \end{bmatrix}, \qquad \text{(A5)}
$$

where the **0** submatrix corresponds to the single and 1–5 type double excitation terms of $\mathbf{T}_{Q,Q}\mathbf{H}_{Q,\mathrm{MC}}$. In other words, if $\mathbf{T}_{Q,Q}\mathbf{H}_{Q,\mathrm{MC}}$ is equivalenced to **A** than the submatrices $\mathbf{A}_{s,\mathrm{MC}}$ and $\mathbf{A}_{d'',\mathrm{MC}}$ are zero where d'' represents the (0,1), (1,0), (1,1), (0,2), and (2,0) subcategories of double excitations.

Of the remaining doubly excited terms all involve core to active excitations. If in addition to removing the semi-internal excitation containing terms from $\mathbf{T}_{Q,Q}\mathbf{H}_{Q,\mathrm{MC}}$ either the core is kept frozen in the calculation or only excitations from the occupied (core plus active) to the virtual orbitals are permitted, then, $\mathbf{T}_{Q,Q}\mathbf{H}_{Q,\mathrm{MC}}$ is zero. This implies that MR-LCCM to MR-CISD comparisons for equivalent configuration sets should be more favorable when either the core is frozen or when all occupied orbitals are treated as active. By neglecting the column vector $\mathbf{T}_{Q,Q}\mathbf{H}_{Q,\mathrm{MC}}$, then, we introduce two possible additional sources of error. The first, which involves the incorrect treatment of semi-internal excitations will become less important as the size of the MCSCF increases (i.e., as the number of reference configurations increase); and the second, is the incorrect handling of the core which is only important if core orbitals are present and not frozen.

[1]W.D. Laidig and R.J. Bartlett, Chem. Phys. Lett. **104**, 424 (1984).
[2]R. J. Bartlett, Annu. Rev. Phys. Chem. **32**, 359 (1981).
[3]B. Jonsson, B.O. Roos, P.R. Taylor, and P.E.M. Seigbahn, J. Chem. Phys. **74**, 4566 (1981).

[4]H. Lischka, R. Shepard, F. B. Brown, and I. Shavitt, Int. J. Quantum Chem. Symp. **15**, 91 (1981).
[5]S. K. Shih, W. Butscher, R. J. Buenker, and S. D. Peyerimhoff, Chem. Phys. **29**, 241 (1978).
[6]P. Saxe, D. J. Fox, and H. F. Schaefer III, J. Chem. Phys. **77**, 5584 (1982).
[7]B. H. Brandow, Rev. Mod. Phys. **39**, 771 (1967).
[8]I. Lindgren, Int. J. Quantum. Chem. Symp. **12**, 33 (1978); I. Lindgren and J. Morrison, *Atomic Many-Body Theory*, Springer Series in Chemical Physics (Springer, Berlin, 1982), Vol. 13.
[9]B. Levy, *Proceedings of the 4th Seminar on Computational Methods in Quantum Chemistry, Orenas, Sweden*, Rep. MPI-PAE/Astro 171, 1978, p. 149.
[10]G. Hose and Kaldor, J. Phys. B **12**, 3927 (1979).
[11]B. Kirtman, J. Chem. Phys. **75**, 798 (1981).
[12]I. Shavitt and L. T. Redmon, J. Chem. Phys. **73**, 5711 (1981).
[13]L. T. Redmon and R. J. Bartlett, J. Chem. Phys. **76**, 1938 (1982).
[14]M. C. Sheppard and K. F. Freed, J. Chem. Phys. **75**, 4507 (1981).
[15]D. Mukherjee, R. K. Moitra, and A. Mukhopadhyay, Pramana **4**, 247 (1975); Mol. Phys. **30**, 1861 (1975); **33**, 955 (1977).
[16]B. Jeziorski and H. Monkhorst, Phys. Rev. A **24**, 1668 (1981).
[17]A. Banerjee and J. Simons, Int. J. Quantum Chem. **19**, 207 (1981).
[18]H. Baker and M. A. Robb, Mol. Phys. **50**, 20 (1983).
[19]K. Tanaka and H. Terashima, Chem. Phys. Lett. **106**, 558 (1984).
[20]I. Lindgren, Phys. Scr. **32**, 291 (1985).
[21]S. A. Kucharski, Y. S. Lee, and R. J. Bartlett (to be published).
[22]U. Kaldor, Phys. Rev. Lett. **31**, 1338 (1973); J. Chem. Phys. **63**, 2199 (1975).
[23]H. Sun and K. F. Freed, Chem. Phys. Lett. **78**, 531 (1981); H. Sun, M. G. Sheppard, and K. F. Freed, *ibid.* **74**, 6842 (1981).
[24]G. Hose and U. Kaldor, Phys. Scr. **21**, 357 (1980); Phys. Rev A **30**, 2932 (1984).
[25]Y. S. Lee and R. J. Bartlett, Int. J. Quantum Chem. Symp. **17**, 347 (1983).
[26]S. Yamamoto and A. Saika, Chem. Phys. Lett. **78**, 316 (1981).
[27]J. Morrison and S. Salomonson, Phys. Scr. **21**, 343 (1980); S. Salomonson, I. Lindgren, and A. M. Martensson, *ibid.* **21**, 351 (1980).
[28]A. Banerjee and J. Simons, J. Chem. Phys. **76**, 4548 (1982).
[29](a) R. J. Bartlett and G. D. Purvis, Int. J. Quantum Chem. **14**, 561 (1978); (b) Phys. Scr. **21**, 255 (1980).
[30]J. Paldus, P. E. S. Wormer, F. Visser, and A. van der Avoird, J. Chem. Phys. **76**, 2458 (1982).
[31]K. Hijikata, Rev. Mod. Phys. **32**, 445 (1960); J. Chem. Phys. **34**, 221, 231 (1961).
[32]Y. S. Lee and R. J. Bartlett, J. Chem. Phys. **80**, 4371 (1984); Y.S. Lee, S.A. Kucharski, and R.J. Bartlett, *ibid.* **81**, 5906 (1984); **82**, 5761(E) (1985).
[33]J. Paldus, in *The Unitary Group for the Evaluation of Electronic Energy Matrix Elements*, edited by J. Hinze, Lecture Notes in Chemistry (Springer, Berlin, 1981), Vol. 22, pp. 1–50; I. Shavitt, *ibid.* pp. 51–99, and references therein.
[34]G. D. Purvis and R. J. Bartlett, J. Chem. Phys. **75**, 1284 (1981).
[35]P. E. S. Wormer, F. Visser, and J. Paldus, J. Comput. Phys. **48**, 23 (1982).
[36]R.J. Bartlett and E.J. Brandas, J. Chem. Phys. **56**, 5467 (1972); **59**, 2032 (1973).
[37]E. R. Davidson, J. Comput. Phys. **17**, 87 (1975).
[38]S. Huzinaga, J. Chem. Phys. **42**, 1293 (1965); T. H. Dunning, *ibid.* **53**, 2823 (1970).
[39]A. Bunge, J. Chem. Phys. **53**, 20 (1970).
[40]In the SDGUGA method removal of the entire spin noninteracting space is quite difficult. The current version of this program only removes a portion of this space.
[41]M.R.A. Blomberg and P.E.M. Siegbahn, Chem. Phys. Lett. **81**, 4 (1981).
[42]L. Brillouin, Act. Sci. Ind. No. 159, Hermann, Paris (1934).
[43]These constants were computed using the program DIAVIB by J. Yates and W. C. Ermler.
[44]The numerical frequencies were computed using a program originally written by K. Kirby-Docken and J. Hinze which was later modified by R. Saxon and others at IBM. This program is described in the article, J. Phys. Chem. **86**, 1305 (1982).
[45]K.P. Huber and G. Herzberg, *Molecular Spectra and Molecular Structure. IV. Constants of Diatomic Molecules* (Van Nostrand Reinhold, New York, 1979).
[46]G. D. Purvis and R. J. Bartlett, J. Chem. Phys. **76**, 1910 (1982).
[47]R.J. Bartlett, H. Sekino, and G.D. Purvis III, Chem. Phys. Lett. **98**, 66 (1983).
[48]H. Schlegel, J. Chem. Phys. **84**, 4530 (1986).
[49]M. Urban, J. Noga, and V. Kello, Theor. Chim. Acta **62**, 549 (1983).
[50]The importance of including the $2\pi_u$ orbital in MCSCF calculations was suggested earlier in the article: G. Das and A. C. Wahl, J. Chem. Phys. **56**, 3532 (1972).
[51]L. T. Redmon, G. D. Purvis, and R. J. Bartlett, J. Am. Chem. Soc. **101**, 2856 (1979).
[52]P. E. M. Siegbahn, Int. J. Quantum Chem. **23**, 1869 (1983).
[53]B. Levy and G. Berthier, Int. J. Quantum Chem. **2**, 307 (1968).
[54]M. Urban, J. Noga, S. J. Cole, and R. J. Bartlett, J. Chem. Phys. **83**, 4041 (1985).
[55]S. J. Cole and R. J. Bartlett (to be published).